On Veracity of Macroscopic Lithium-Ion Battery Models

Harikesh Arunachalam,[a,z] Simona Onori,[a] and Ilenia Battiato[b]

[a]*Clemson University International Center for Automotive Research, Greenville, South Carolina 29607, USA*
[b]*Department of Mechanical Engineering, San Diego State University, San Diego, California 92182, USA*

Batteries are electrochemical energy storage devices that exhibit physico-chemical heterogeneity on a continuity of scales. As such, battery systems are amenable to mathematical descriptions on a multiplicity of scales that range from atomic to continuum. In this paper we present a new method to assess the veracity of macroscopic models of lithium-ion batteries. Macroscopic models treat the electrode as a continuum and are often employed to describe the mass and charge transfer of lithium since they are computational tractable and practical to model the system at the cell scale. Yet, they rely on a number of simplifications and assumptions that may be violated under given operating conditions. We use multiple-scale expansions to upscale the pore-scale Poisson-Nerst-Planck (PNP) equations and establish sufficient conditions under which macroscopic dual-continua mass and charge transport equations accurately represent pore-scale dynamics. We propose a new method to quantify the relative importance of three key pore-scale transport mechanisms (electromigration, diffusion and heterogenous reaction) by means of the electric Péclet (Pe) and Damköhler (Da) numbers in the electrolyte and the electrode phases. For the first time, applicability conditions of macroscopic models through a phase diagram in the (Da-Pe)-space are defined. Finally, we discuss how the new proposed tool can be used to assess the validity of macroscopic models across different battery chemistry and conditions of operation. In particular, a case study analysis is presented using commercial lithium-ion batteries that investigates the validity of Newman-type macroscopic models under temperature and current rate of charge/discharge variation.
 [DOI: 10.1149/2.0771509jes]

Manuscript submitted February 2, 2015; revised manuscript received June 11, 2015. Published July 16, 2015.

Predictive understanding of battery dynamical behavior still remains a major bottleneck in achieving diagnostic capabilities, safety, optimization and control of battery systems under different operating conditions. Such a difficulty arises from two main factors: i) nonlinearity of lithium-ion transport processes[1] and ii) battery systems multiscale structure that exhibits physicochemical heterogeneity on a continuity of scales (from the nanometer to the meter).[2–5] Since the seminal work by Newman and Tiedemann,[6] where macroscopic ion transport equations were first formulated, a plethora of models have spurred in the past decades. They range from fully empirical approaches to generalizations of electrochemical models based on the porous electrode theory to account for concentrated solutions,[7,8] thermal effects[9] and capacity fade due to Solid-Electrolyte Interphase (SEI)-growth,[10–12] just to mention a few. In the past decade, ever increasing computational capabilities have fuelled the development of fully molecular/atomistic models and multiscale/multiphysics approaches.[13] For a thorough review on the topic, we refer the reader to Ref. 4.

Microscale models[14,15] (e.g. molecular dynamics, kinetic Monte Carlo and pore-scale models) are theoretically robust, but are impractical as a predictive tool at the system level due to their computational burden. For example, current molecular dynamics simulations are still prohibitive at the nano-second timescale.[4,16] Such computational limitations become dire when modeling battery lifetime and slow degradation processes over hundreds or thousands of cycles. Further, the need for real-time estimation of battery State-of-Charge (SOC) and State-of-Health (SOH) currently limits the application of more accurate and computationally intensive models in favor of simpler macroscopic (effective, coarse-grained, continuum, etc.)[17,18] and/or reduced-order representations.[19,20]

Macroscopic approaches overcome some of the computational challenges of microscale models by relying on a number of closure assumptions and/or phenomenological descriptions such as geometrical constraints that guarantee scale separation between the pore- and the continuum-scales, linearization of pore-scale equations, etc. These are often necessary to fully decouple micro-scale descriptions from their continuum counterpart. Yet, physical and electrochemical phenomena on one scale (e.g. particle-scale) affect, and are often coupled to, phenomena on a vastly different scale (e.g. cell-scale).[21–23] For example, pore-scale molecular diffusion fundamentally affects lithium-ion mixing and heat generation at the electrode scale,[9] and localized SEI-growth in the pores (over time scales spanning many orders of magnitude) can lead to drastic porosity changes and long term impairment (e.g. aging and capacity fade) of battery systems. Further, dependence of battery aging processes on usage patterns[20,24] (i.e. charge and dischrage cycles amplitude and frequency) are often symptoms of coupled dynamics *across* scales.[25]

Upscaling techniques - e.g. volume-averaging,[26] homogenization[27] and its generalization to evolving microstructures,[28] thermodynamically-constrained averaging[29] and renormalization group theory[30] - allow one to relate pore-scale processes to their continuum counterparts. An increasing number of studies have focused on the formal derivation of continuum-scale models from micro-scale balance equations.[31–35] These studies reflect the need to validate reduced-order models and to elucidate the macroscopic response of microscale processes. Yet, to the best of our knowledge, no current work has rigorously established the conditions under which pore-scale equations describing electromigration, diffusion and reaction of lithium ions correctly upscale to the classical macroscopic porous-electrode equations. The identifications of conditions under which continuum approaches are a valid representation of microscopic processes is critical to achieve model predictivity of battery systems.

Following the approach introduced by,[22,23] we use multiple-scale expansions technique to upscale the dimensionless PNP equations describing lithium dynamics and to derive physics-based conditions under which classical porous-electrode continuum models, or dual-continua diffusion-migration-reaction (DMR) equations, accurately describe lithium-ion pore-scale dynamics.

The paper is structured as follows. First, we present the pore-scale isothermal transport model of lithium ions subject to diffusion and electromigration in the electrode and electrolyte phases, and heterogenous Butler-Volmer kinetic reaction at the electrode-electrolyte interface. Then, we formulate the problem in dimensionless form and identify the Damköhler (Da) and electric Péclet (Pe) numbers as parameters that control lithium-ion transport processes (i.e. diffusion, electromigration and reaction) in the electrode and electrolyte. We employ multiple-scale expansions to derive effective (macroscopic) dual-continua DMR equations and rigorously identify conditions under which such a continuum approximation breaks down. The region of validity of the continuum description is graphically represented by two phase diagrams in the (Da, Pe) space for the electrode and the electrolyte phases. Then, we discuss the implications of our findings on the classical porous-electrode model proposed by Doyle and

[z]E-mail: harunac@clemson.edu

Newman.[8] Lastly, we present a case study analysis to investigate the validity of macroscale models in relations to: 1) different chemistry, and 2) different conditions of operation in terms of temperature and C-rate for a series of commercially available batteries. We achieve this by relating macroscale models' predictive performance to the applicability regimes. Finally, we conclude with a summary of our results.

Pore-Scale Governing Equations

We consider the microscale transport of lithium ions in a battery electrode constituted of a porous matrix $\hat{\Omega}$ with characteristic length L. Let us assume that the active particles are microscopically arranged in the medium in the form of spatially periodic unit cells $\hat{Y}$ with a characteristic length ℓ. We define the characteristic length ℓ as the diameter of the spherical active particles and ε as the scale-separation parameter $\varepsilon \equiv \ell/L \ll 1$. The unit cell $\hat{Y} = \hat{\mathcal{B}} \cup \hat{\mathcal{S}}$ consists of the electrolyte space $\hat{\mathcal{B}}$ and the ion permeable solid matrix $\hat{\mathcal{S}}$, separated by the smooth surface $\hat{\Gamma}$. The pore spaces $\hat{\mathcal{B}}$ of each cell $\hat{Y}$ form a multi-connected pore-space domain $\hat{\mathcal{B}}^\varepsilon \subset \hat{\Omega}$ bounded by the smooth surface $\hat{\Gamma}^\varepsilon$.

The mass and charge transport equations in the electrolyte and the electrode phases control the spatiotemporal evolution of the concentration of lithium ions $\hat{c}_\varepsilon^i(\mathbf{x}, t)$ $(\text{mol} \cdot \text{m}^{-3})$ and the electrostatic potential $\hat{\phi}_\varepsilon^i(\mathbf{x}, t)$ (V) in the active particles $\{i = s\}$ and the electrolyte $\{i = e\}$. For completeness, we summarize the set of governing equations in the following sections.

Electrolyte phase.— The mass and charge transport equations in the electrolyte phase $\mathbf{x} \in \hat{\mathcal{B}}^\varepsilon$ are[36]

$$\frac{\partial \hat{c}_\varepsilon^e}{\partial \hat{t}} = \hat{\nabla} \cdot [(\hat{\mathbf{D}}^e + \lambda t_+^2 RTF^{-2}\hat{\mathbf{K}}^e/\hat{c}_\varepsilon^e)\hat{\nabla}\hat{c}_\varepsilon^e + t_+ F^{-1}\hat{\mathbf{K}}^e\hat{\nabla}\hat{\phi}_\varepsilon^e], \quad [1a]$$

$$0 = \hat{\nabla} \cdot [(\lambda t_+ RTF^{-1}\hat{\mathbf{K}}^e/\hat{c}_\varepsilon^e)\hat{\nabla}\hat{c}_\varepsilon^e + \hat{\mathbf{K}}^e\hat{\nabla}\hat{\phi}_\varepsilon^e], \quad [1b]$$

subject to

$$\mathbf{n}_e \cdot [(\hat{\mathbf{D}}^e + \lambda t_+^2 RTF^{-2}\hat{\mathbf{K}}^e/\hat{c}_\varepsilon^e)\hat{\nabla}\hat{c}_\varepsilon^e + t_+ F^{-1}\hat{\mathbf{K}}^e\hat{\nabla}\hat{\phi}_\varepsilon^e] = kF^{-1}\hat{f}(\hat{c}_\varepsilon^e, \hat{c}_\varepsilon^s, \hat{\phi}_\varepsilon^s, \hat{\phi}_\varepsilon^e), \quad [2a]$$

$$\mathbf{n}_e \cdot [(\lambda t_+ RTF^{-1}\hat{\mathbf{K}}^e/\hat{c}_\varepsilon^e)\hat{\nabla}\hat{c}_\varepsilon^e + \hat{\mathbf{K}}^e\hat{\nabla}\hat{\phi}_\varepsilon^e] = k\hat{f}(\hat{c}_\varepsilon^e, \hat{c}_\varepsilon^s, \hat{\phi}_\varepsilon^s, \hat{\phi}_\varepsilon^e), \quad [2b]$$

on the solid-electrolyte boundary Γ^ε, respectively. In (2),

$$\hat{f}(\hat{c}_\varepsilon^e, \hat{c}_\varepsilon^s, \hat{\phi}_\varepsilon^s, \hat{\phi}_\varepsilon^e) = 2\sqrt{\hat{c}_\varepsilon^e \hat{c}_\varepsilon^s (1 - \hat{c}_\varepsilon^s/\hat{c}_{\max}^s)} \cdot \sinh[F(\hat{\phi}_\varepsilon^s - \hat{\phi}_\varepsilon^e - \hat{U})/2RT] \quad [3]$$

$\hat{\mathbf{D}}^e$ $(\text{m}^2\text{sec}^{-1})$ and $\hat{\mathbf{K}}^e$ $(\Omega^{-1}\text{m}^{-1})$ are the interdiffusion coefficient and the electric conductivity in the electrolyte, respectively; k $(\text{A} \cdot \text{m} \cdot \text{mol}^{-1})$ is the electrochemical reaction rate constant that describes the kinetics of lithium-ion transfer on Γ^ε; $\hat{U}$ (V) is the open circuit potential; $\hat{c}_{\max}^s$ is the maximum concentration of lithium that can be stored in the active particle; t_+ is the transference number, $\lambda := 1 + \frac{\text{d} \ln f_\pm}{\text{d} \ln(\hat{c}_\varepsilon^e/\hat{c}_{\max}^s)}$ is assumed constant,[37] and $f_\pm$ is the activity coefficient; $\mathbf{n}_e$ is the outward unit normal vector to $\hat{\Gamma}^\varepsilon$ pointing from the electrolyte toward the active particle; F and R are the Faraday and the universal gas constants; T is temperature.

Electrode phase.— The mass and charge transport of lithium ions in the electrode (solid) phase $\hat{\mathcal{S}}^\varepsilon$ are governed by the material balance and electroneutrality equations[36]

$$\frac{\partial \hat{c}_\varepsilon^s}{\partial \hat{t}} = \hat{\nabla} \cdot (\hat{\mathbf{D}}^s \hat{\nabla}\hat{c}_\varepsilon^s), \quad \hat{\mathbf{x}} \in \hat{\mathcal{S}}^\varepsilon, \quad [4a]$$

$$0 = \hat{\nabla} \cdot (\hat{\mathbf{K}}^s \hat{\nabla}\hat{\phi}_\varepsilon^s), \quad \hat{\mathbf{x}} \in \hat{\mathcal{S}}^\varepsilon, \quad [4b]$$

subject to

$$-\mathbf{n}_s \cdot (\hat{\mathbf{D}}^s \hat{\nabla}\hat{c}_\varepsilon^s) = kF^{-1}\hat{f}(\hat{c}_\varepsilon^e, \hat{c}_\varepsilon^s, \hat{\phi}_\varepsilon^s, \hat{\phi}_\varepsilon^e), \quad \hat{\mathbf{x}} \in \hat{\Gamma}^\varepsilon \quad [5a]$$

$$-\mathbf{n}_s \cdot (\hat{\mathbf{K}}^s \hat{\nabla}\hat{\phi}_\varepsilon^s) = k\hat{f}(\hat{c}_\varepsilon^e, \hat{c}_\varepsilon^s, \hat{\phi}_\varepsilon^s, \hat{\phi}_\varepsilon^e), \quad \hat{\mathbf{x}} \in \hat{\Gamma}^\varepsilon \quad [5b]$$

respectively. In (4)-(5), $\hat{\mathbf{D}}^s$ $(\text{m}^2\text{sec}^{-1})$ is the interdiffusion coefficient in the electrode, $\hat{\mathbf{K}}^s$ $(\Omega^{-1}\text{m}^{-1})$ is the electric conductivity in the electrode, and $\mathbf{n}_s$ is the outward unit normal vector to Γ^ε pointing from the active particle toward the electrolyte.

Dimensionless Formulation

Transport processes and dimensionless numbers.— The transport processes occurring at the pore-scale include heterogenous reaction on the electrode-electrolyte interface $\hat{\Gamma}^\varepsilon$, and diffusion and migration in the electrode and electrolyte phases, $\hat{\mathcal{S}}^\varepsilon$ and $\hat{\mathcal{B}}^\varepsilon$, respectively. The characteristic time scales associated with the heterogenous reaction, ionic diffusion, and ionic migration over a macroscopic length scale L are

$$\hat{t}_R = \frac{LF}{k}, \quad \hat{t}_{D_j} = \frac{L^2}{D^i}, \quad \hat{t}_{M_j} = \frac{F^2 L^2 \hat{c}_{\max}^s}{RTK^j}, \quad j = \{e, s\}, \quad [6]$$

respectively. In (6), $D^j = \mathcal{O}(\hat{\mathbf{D}}^j)$ and $K^j = \mathcal{O}(\hat{\mathbf{K}}^j)$, $j = \{e, s\}$, are characteristic values of the interdiffusion and electric conductivity tensors $\hat{\mathbf{D}}^j$ and $\hat{\mathbf{K}}^j$ in the electrode $(j = s)$ and the electrolyte $(j = e)$, respectively. We define the dimensionless Damköhler and electric Péclet numbers as

$$\text{Da}_j := \frac{\hat{t}_{D_j}}{\hat{t}_R} = \frac{Lk}{FD^j} \quad \text{and} \quad \text{Pe}_j := \frac{\hat{t}_{D_j}}{\hat{t}_{M_j}} = \frac{RTK^j}{F^2 D^j \hat{c}_{\max}^s}, \quad j = \{e, s\}. \quad [7]$$

They provide information about the relative magnitude of ion transport processes in the electrolyte and the electrode phases. Let $c_\varepsilon^j := \hat{c}_\varepsilon^j/\hat{c}_{\max}^s$ and $\phi_\varepsilon^j := \hat{\phi}_\varepsilon^j F/(2RT)$, $j = \{s, e\}$ be the dimensionless lithium-ion concentration and electrostatic potential in the active particles $(j = s)$ and the electrolyte $(j = e)$. Then, the mass and charge transport equations can be cast in dimensionless form as follows.

Electrolyte phase.— The dimensionless form of mass and charge transport in the electrolyte (1)-(2) is given by

$$\frac{\partial c_\varepsilon^e}{\partial t} = \nabla \cdot [(\mathbf{D}^e + \lambda t_+^2 \text{Pe}_e \mathbf{K}^e/c_\varepsilon^e)\nabla c_\varepsilon^e + 2\text{Pe}_e t_+ \mathbf{K}^e \nabla\phi_\varepsilon^e], \quad \mathbf{x} \in \mathcal{B}^\varepsilon \quad [8a]$$

$$0 = \nabla \cdot [(\lambda t_+ \mathbf{K}^e/c_\varepsilon^e)\nabla c_\varepsilon^e + 2\mathbf{K}^e\nabla\phi_\varepsilon^e], \quad \mathbf{x} \in \mathcal{B}^\varepsilon \quad [8b]$$

subject to

$$\mathbf{n}_e \cdot [(\mathbf{D}^e + \lambda t_+^2 \text{Pe}_e \mathbf{K}^e/c_\varepsilon^e)\nabla c_\varepsilon^e + 2\text{Pe}_e\, t_+ \mathbf{K}^e \nabla\phi_\varepsilon^e] = \text{Da}_e f(c_\varepsilon^e, c_\varepsilon^s, \phi_\varepsilon^s, \phi_\varepsilon^e), \quad [9a]$$

$$\mathbf{n}_e \cdot [(\text{Pe}_e \lambda t_+ \mathbf{K}^e/c_\varepsilon^e)\nabla c_\varepsilon^e + 2\text{Pe}_e \mathbf{K}^e \nabla\phi_\varepsilon^e] = \text{Da}_e f(c_\varepsilon^e, c_\varepsilon^s, \phi_\varepsilon^s, \phi_\varepsilon^e), \quad [9b]$$

on Γ^ε, respectively. In (1) and (2), the dimensional spatial and time scales are nondimensionalized by the macroscopic length L and the diffusion time in the electrolyte phase $\hat{t}_{D_e}$ respectively, i.e. $\mathbf{x} = \hat{\mathbf{x}}/L$ and $t_e = \hat{t}/\hat{t}_{D_e}$; $\mathbf{D}^e = \hat{\mathbf{D}}^e/D^e$ and $\mathbf{K}^e = \hat{\mathbf{K}}^e/K^e$ are the dimensionless interdiffusion coefficient and the electric conductivity in the electrolyte. Also,

$$f(c_\varepsilon^e, c_\varepsilon^s, \phi_\varepsilon^e, \phi_\varepsilon^s) = 2\sqrt{c_\varepsilon^e c_\varepsilon^s (1 - c_\varepsilon^s)}\sinh(\phi_\varepsilon^s - \phi_\varepsilon^e - U) \quad [10]$$

where $U = F\hat{U}/(2RT)$ is the dimensionless open circuit potential. We emphasize that $\mathcal{B}^\varepsilon$ and $\mathcal{S}^\varepsilon$ represent the rescaled (nondimensional) electrolyte and electrode phases, with Γ^ε the interface separating them.

Electrode phase.— Similarly, the dimensional transport equations in the electrode phase $\mathbf{x} \in \hat{\mathcal{S}}^\varepsilon$, (4) and (5), can be cast in dimensionless

form

$$\frac{\partial c_\varepsilon^s}{\partial t} = \mathrm{Da}_e \mathrm{Da}_s^{-1} \nabla \cdot (\mathbf{D}^s \nabla c_\varepsilon^s), \quad \mathbf{x} \in \mathcal{S}^\varepsilon, \tag{11a}$$

$$0 = \nabla \cdot (\mathbf{K}^s \nabla \phi_\varepsilon^s), \quad \mathbf{x} \in \mathcal{S}^\varepsilon, \tag{11b}$$

subject to

$$-\mathbf{n}_s \cdot (\mathbf{D}^s \nabla c_\varepsilon^s) = \mathrm{Da}_s f(c_\varepsilon^e, c_\varepsilon^s, \phi_\varepsilon^s, \phi_\varepsilon^e), \quad \mathbf{x} \in \Gamma^\varepsilon, \tag{12a}$$

$$-\mathbf{n}_s \cdot (2\mathrm{Pe}_s \mathbf{K}^s \nabla \phi_\varepsilon^s) = \mathrm{Da}_s f(c_\varepsilon^e, c_\varepsilon^s, \phi_\varepsilon^s, \phi_\varepsilon^e), \quad \mathbf{x} \in \Gamma^\varepsilon, \tag{12b}$$

respectively.

In the following we use multiple-scale expansions to derive a mean-field (continuum, macroscopic) approximation of the pore-scale equations and to identify conditions under which continuum equations are valid descriptors of pore-scale dynamics.

Homogenization via Multiple-Scale Expansions

We define the following local averages of a quantity $\mathcal{A}(\mathbf{x})$

$$\langle \mathcal{A} \rangle_e \equiv \frac{1}{|Y|} \int_{\mathcal{B}(\mathbf{x})} \mathcal{A} \mathrm{d}\mathbf{y}, \quad \langle \mathcal{A} \rangle_s \equiv \frac{1}{|Y|} \int_{\mathcal{S}(\mathbf{x})} \mathcal{A} \mathrm{d}\mathbf{y}, \tag{13}$$

$$\langle \mathcal{A} \rangle_\mathcal{B} \equiv \frac{1}{|\mathcal{B}|} \int_{\mathcal{B}(\mathbf{x})} \mathcal{A} \mathrm{d}\mathbf{y}, \quad \langle \mathcal{A} \rangle_\mathcal{S} \equiv \frac{1}{|\mathcal{S}|} \int_{\mathcal{S}(\mathbf{x})} \mathcal{A} \mathrm{d}\mathbf{y}, \tag{14}$$

$$\langle \mathcal{A} \rangle_\Gamma \equiv \frac{1}{|\Gamma|} \int_{\Gamma(\mathbf{x})} \mathcal{A} \mathrm{d}\mathbf{y}, \tag{15}$$

where $\langle \mathcal{A} \rangle_e = \eta \langle \mathcal{A} \rangle_\mathcal{B}$, $\langle \mathcal{A} \rangle_s = (1-\eta)\langle \mathcal{A} \rangle_\mathcal{S}$ and $\eta = |\mathcal{B}|/|Y|$ is the electrode porosity. Using the method of multiple-scale expansions, we introduce a fast space variable $\mathbf{y}$ defined in the unit cell Y, $\mathbf{y} \in Y$, and three time variables. One of the three time variables is related to reaction τ_r and two to migration $[\boldsymbol{\tau}_\mathrm{m}]_j = \tau_{\mathrm{m}j}$ in the electrolyte and the active particles $j = \{e, s\}$, respectively

$$\begin{aligned} \mathbf{y} &:= \varepsilon^{-1}\mathbf{x}, \quad \tau_\mathrm{r} := \hat{t}_R^{-1}\hat{t} = \mathrm{Da}_e t, \\ \tau_{\mathrm{m}j} &:= \hat{t}_{M_j}^{-1}\hat{t} = \mathrm{Pe}_j \mathrm{Da}_e \mathrm{Da}_j^{-1} t, \quad j = \{e, s\} \end{aligned} \tag{16}$$

where $t = \hat{t}/\hat{t}_{D_e}$ is a dimensionless time. No Einstein notation convention is implied if a repeated index is present. Replacing any pore scale quantity $\psi_\varepsilon(\mathbf{x}, t)$ (e.g. concentration, electrostatic potential in either phase) with $\psi(\mathbf{x}, \mathbf{y}, t, \tau_\mathrm{r}, \boldsymbol{\tau}_\mathrm{m})$ provides the following relations for the space and time derivatives,

$$\nabla \psi_\varepsilon = \nabla_\mathbf{x} \psi + \varepsilon^{-1} \nabla_\mathbf{y} \psi \tag{17a}$$

$$\frac{\partial \psi_\varepsilon}{\partial t} = \frac{\partial \psi}{\partial t} + \mathrm{Da}_e \frac{\partial \psi}{\partial \tau_\mathrm{r}} + \mathrm{Pe}_e \left(\frac{\partial \psi}{\partial \tau_{\mathrm{m}e}} + \frac{\mathrm{Da}_e}{\mathrm{Da}_s} \frac{\partial \psi}{\partial \tau_{\mathrm{m}s}} \right). \tag{17b}$$

Additionally, we represent ψ as an asymptotic series in integer powers of ε

$$\psi(\mathbf{x}, \mathbf{y}, t, \tau_\mathrm{r}, \boldsymbol{\tau}_\mathrm{m}) = \sum_{n=0}^{\infty} \varepsilon^n \psi_n(\mathbf{x}, \mathbf{y}, t, \tau_\mathrm{r}, \boldsymbol{\tau}_\mathrm{m}), \tag{18}$$

where ψ_n, $n = \{0, 1, \cdots\}$ are Y-periodic functions in $\mathbf{y}$. Finally, we set

$$\mathrm{Pe}_e = \varepsilon^{-\alpha}, \quad \mathrm{Da}_e = \varepsilon^\beta, \quad \mathrm{Da}_s = \varepsilon^\gamma, \quad \mathrm{Pe}_s = \varepsilon^{-\delta} \tag{19}$$

where the exponents α, β, γ and δ determine the system behavior in the electrolyte and electrode phases.

Upscaled transport equations in the electrolyte.— Lithium transport in the electrolyte phase described by (8a)–(9b) can be homogenized, i.e., approximated up to order ε^2, by the following effective mass and charge transport equations (see Appendix A)

$$\begin{aligned} \eta \partial_t \langle c^e \rangle_\mathcal{B} = \nabla_\mathbf{x} \cdot [&(\mathbf{D}^{e\star\star} + \varepsilon^{-\alpha} \lambda t_+^2 \mathbf{K}^{e\star\star} / \langle c^e \rangle_\mathcal{B}) \nabla_\mathbf{x} \langle c^e \rangle_\mathcal{B} \\ &+ 2\mathrm{Pe}_e t_+ \mathbf{K}^{e\star\star} \nabla_\mathbf{x} \langle \phi^e \rangle_\mathcal{B}] \\ &+ 2\eta \varepsilon^{-1} \mathcal{K}^\star \mathrm{Da}_e f(\langle c^e \rangle_\mathcal{B}, \langle c^s \rangle_s, \langle \phi^e \rangle_\mathcal{B}, \langle \phi^s \rangle_s), \end{aligned} \tag{20}$$

and

$$\begin{aligned} \mathrm{Pe}_e \nabla_\mathbf{x} \cdot [&(\lambda t_+ \mathbf{K}^{e\star\star} / \langle c^e \rangle_\mathcal{B}) \nabla_\mathbf{x} \langle c^e \rangle_\mathcal{B} + 2\mathbf{K}^{e\star\star} \nabla_\mathbf{x} \langle \phi^e \rangle_\mathcal{B}] \\ &= 2\eta \varepsilon^{-1} \mathcal{K}^\star \mathrm{Da}_e f(\langle c^e \rangle_\mathcal{B}, \langle c^s \rangle_s, \langle \phi^e \rangle_\mathcal{B}, \langle \phi^s \rangle_s), \end{aligned} \tag{21}$$

where

$$\begin{aligned} &f(\langle c^e \rangle_\mathcal{B}, \langle c^s \rangle_s, \langle \phi^e \rangle_\mathcal{B}, \langle \phi^s \rangle_s) \\ &= 2\sqrt{\langle c^e \rangle_\mathcal{B} \langle c^s \rangle_s (1 - \langle c^s \rangle_s)} \sinh(\langle \phi^s \rangle_s - \langle \phi^e \rangle_\mathcal{B} - U) \end{aligned} \tag{22}$$

provided the following conditions are met:

1) $\varepsilon \ll 1$,
2) $\mathrm{Da}_e < 1$,
3) $\mathrm{Pe}_e < 1$,
4) $\mathrm{Da}_e/\mathrm{Pe}_e < 1$,
5) $\langle \boldsymbol{\chi}^e \rangle_\Gamma \approx \langle \boldsymbol{\chi}^e \rangle_\mathcal{B}$.

In (20) and (21), the dimensionless effective reaction rate constant in the electrolyte phase, $\mathcal{K}^\star$, is determined by the pore geometry,

$$\mathcal{K}^\star = \frac{|\Gamma|}{|\mathcal{B}|}, \tag{23}$$

and the dispersion tensors are given by:

$$\begin{aligned} \mathbf{D}^{e\star\star} &= \langle \mathbf{D}^e (\mathbf{I} + \nabla_\mathbf{y} \boldsymbol{\chi}^e) \rangle_e, \\ \mathbf{K}^{e\star\star} &= \langle \mathbf{K}^e (\mathbf{I} + \nabla_\mathbf{y} \boldsymbol{\chi}^e) \rangle_e, \end{aligned} \tag{24}$$

The closure variable $\boldsymbol{\chi}^e(\mathbf{y})$ has zero mean, $\langle \boldsymbol{\chi}^e \rangle_e = \mathbf{0}$, and is defined as a solution to the local problem

$$\nabla_\mathbf{y} \cdot (\nabla_\mathbf{y} \boldsymbol{\chi}^e + \mathbf{I}) = 0, \quad \mathbf{y} \in \mathcal{B}, \tag{25a}$$

$$\mathbf{n}_e \cdot (\nabla_\mathbf{y} \boldsymbol{\chi}^e + \mathbf{I}) = 0, \quad \mathbf{y} \in \Gamma. \tag{25b}$$

Constraints 1)–4) ensure separation of scales. While constraint 1) is almost always met in practical applications since the pore size is generally much smaller that the electrode dimension, constraints 2)–4) depend on the relative importance of the diffusion, electromigration, and reaction mechanisms, i.e. they impose constraints on the transport regimes that can be appropriately modeled by the continuum scale Equations (20) and (21) within errors of order ε^2. These conditions are summarized in the phase diagram in Figure 1, where the line $\beta = 0$ refers to $\mathrm{Da}_e = 1$ and the half-space $\beta > 0$ refers to $\mathrm{Da}_e < 1$ because $\varepsilon < 1$; the line $\alpha = 0$ refers to $\mathrm{Pe}_e = 1$ and the half-space $\alpha_e < 0$ refers to $\mathrm{Pe}_e < 1$; the line $\alpha + \beta = 0$ refers to $\mathrm{Da}_e/\mathrm{Pe}_e = 1$; and the half-space underneath this line refers to $\mathrm{Da}_e/\mathrm{Pe}_e < 1$. Constraint 5) is not necessary for scale separation, but facilitates the derivation of the effective parameters (23) and (24). As shown in Appendix A, this constraint allows one to interchange the surface and volume averages, $\langle c_1^e \rangle_\Gamma \approx \langle c_1^e \rangle_\mathcal{B}$ and $\langle \phi_1^e \rangle_\Gamma \approx \langle \phi_1^e \rangle_\mathcal{B}$, within errors on the order of ε^2.

Upscaled transport equations in the electrode.— In Appendix B, we show that the microscale reactive transport processes described by (11)–(12) can be homogenized, i.e., approximated up to order ε^2 in the solid phase with an effective mass and charge transport equations

$$\partial_t \langle c^s \rangle_s = \nabla_\mathbf{x} \cdot (\mathbf{D}^{s\star\star} \nabla_\mathbf{x} \langle c^s \rangle_s) - \varepsilon^{-1} \eta \mathrm{Da}_s \mathcal{K}^\star f(\langle c^e \rangle_\mathcal{B}, \langle c^s \rangle_s, \langle \phi^e \rangle_\mathcal{B}, \langle \phi^s \rangle_s), \tag{26}$$

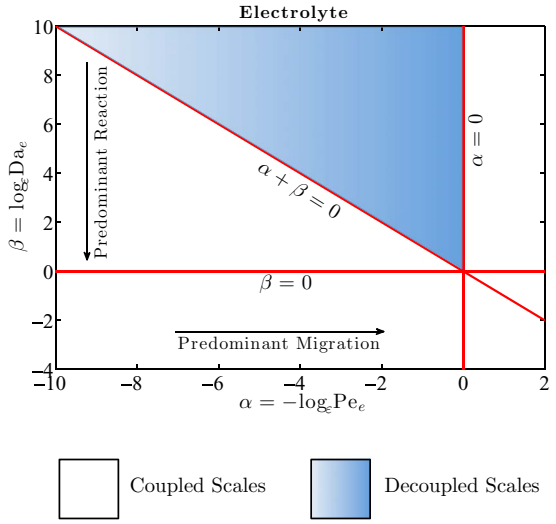

Figure 1. Phase diagram specifying the range of applicability of the upscaled Equations (20) and (21) for the diffusion-migration-reaction of lithium ions in the electrolyte in terms of Pe_e and Da_e. The gray region identifies the conditions under which the macro-scale Equations (20) and (21) hold. In the white region, micro- and macro-scale equations are coupled and need to be solved simultaneously. Diffusion, migration, and reaction are of the same order of magnitude at the point $(\alpha, \beta) = (0, 0)$.

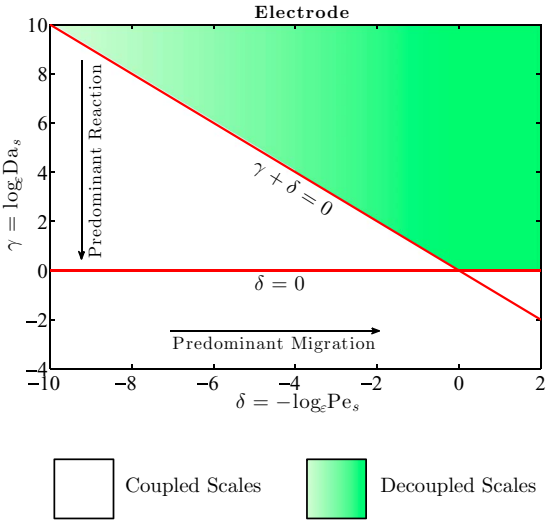

Figure 2. Phase diagram specifying the range of applicability of the upscaled Equations (26) and (27) for the diffusion-reaction of lithium ions in the electrode in terms of Pe_s and Da_s. The gray region identifies the conditions under which the macro-scale Equations (26) and (27) hold. In the white region, micro- and macro-scale equations are coupled and need to be solved simultaneously. Diffusion and reaction are of the same order of magnitude at the point $(\delta, \gamma) = (0, 0)$.

and

$$2\mathrm{Pe}_s \nabla_{\mathbf{x}} \cdot (\mathbf{K}^{s\star\star} \nabla_{\mathbf{x}} \langle \phi^s \rangle_s) = \varepsilon^{-1} \eta \mathrm{Da}_s \mathcal{K}^\star f(\langle c^e \rangle_{\mathcal{B}}, \langle c^s \rangle_s, \langle \phi^e \rangle_{\mathcal{B}}, \langle \phi^s \rangle_s), \quad [27]$$

for $\mathbf{x} \in \Omega$, provided the additional conditions

1) $\mathrm{Da}_s < 1$,
2) $\mathrm{Da}_s/\mathrm{Pe}_s < 1$,
3) $\langle \boldsymbol{\chi}^s \rangle_\Gamma \approx \langle \boldsymbol{\chi}^s \rangle_s$,

are met. In (26) and (27), the dimensionless parameter $\mathcal{K}^\star$ is defined by (23) and the effective diffusion and conductivity tensors are given by

$$\mathbf{D}^{s\star\star} = \langle \mathbf{D}^s (\mathbf{I} + \nabla_{\mathbf{y}} \boldsymbol{\chi}^s) \rangle_s,$$
$$\mathbf{K}^{s\star\star} = \langle \mathbf{K}^s (\mathbf{I} + \nabla_{\mathbf{y}} \boldsymbol{\chi}^s) \rangle_s. \quad [28]$$

The closure variable $\boldsymbol{\chi}^s(\mathbf{y})$ has zero mean, $\langle \boldsymbol{\chi}^s \rangle_s = \mathbf{0}$, and is defined as a solution of the local problem

$$\nabla_{\mathbf{y}} \cdot [\mathbf{D}^s (\mathbf{I} + \nabla_{\mathbf{y}} \boldsymbol{\chi}^s)] = 0, \quad \mathbf{y} \in \mathcal{S}, \quad [29a]$$

$$\mathbf{n}_s \cdot [\mathbf{D}^s (\mathbf{I} + \nabla_{\mathbf{y}} \boldsymbol{\chi}^s)] = 0, \quad \mathbf{y} \in \Gamma. \quad [29b]$$

Constraints 1)–2) ensure scales separation and depend on the relative importance of the solid phase diffusion, conduction, and reaction mechanisms of transport. Condition 3) simply facilitates the derivation of the effective tensor (28). These constraints are summarized in Figure 2.

Physical interpretation of applicability conditions of macroscopic models.— The constraints previously identified impose conditions on the relative magnitude of the three main processes controlling lithium-ion transport at the microscale, i.e. diffusion, electromigration and heterogenous reaction at the electrolyte-electrode interface. The constraints $\mathrm{Da}_e < 1$ and $\mathrm{Da}_s < 1$ require that the intercalation reaction be slower than diffusion processes both in the electrolyte and the electrode. Similarly $\mathrm{Pe}_e < 1$ requires that diffusion processes in the electrolyte are faster than elecromigration. Both conditions guarantee that lithium ions are uniformly distributed, i.e. well mixed, both in the pore-space occupied by the electrolyte and within electrode pellets at the unit cell scale. Under well-mixed conditions, or when lithium-ion concentration is locally uniform, a dual-continua macroscale model can describe processes at the micro-scale within errors of order $\mathcal{O}(\varepsilon^2)$ as prescribed by the homogenization procedure. On the other hand, under diffusion-limited conditions, or high resistance to mass transport, concentration gradients are formed at the sub-pore scale, and the predictivity of continuum scale models, which replace pore-scale quantities with their spatial averages, cannot be guaranteed any longer. Our findings are consistent with the widespread observation that classical macroscopic approximations loose predictive power under high C-rate[c] operating conditions,[39] when a strong current imbalance between electrodes generates sharp concentration gradients at the sub pore level. The importance of lack of subpore scale mixing was already pointed out in Ref. 9, where subgrid concentration gradients were associated with generation of highly localized heat of mixing. The constraints $\mathrm{Da}_e/\mathrm{Pe}_e < 1$ and $\mathrm{Da}_s/\mathrm{Pe}_s < 1$ suggest that elecromigration can play a favorable role in improving the sub-pore scale mixing in presence of high mass transfer resistance, or diffusion-limited regimes. Finally, the dependence of Pe_e and Pe_s on the operating temperature, see (7), demonstrates that isothermal conditions are not sufficient to guarantee macroscale model accuracy: operating the same battery at a higher temperature may lead to the violation of $\mathrm{Pe}_e < 1$ and/or $\mathrm{Pe}_s < 1$, once a critical temperature is overcome. A more thorough analysis of temperature-dependent breakdown for different battery chemistry is discussed in the next section as well as in Ref. 40. In the following section, we discuss the implications of our findings on existing dual continua models.

Implications on Existing Macroscale Models for SOC and SOH Estimation

A number of works have focused on control strategies and SOH/SOC estimation based on electrochemical models.[39,41,42] Some

[c]C-rate is defined as the rate of charge or discharge current in normalized form:

$$\text{C-rate} = \frac{I}{Q_{nom}} [1/\mathrm{h}]$$

where I is the battery current and Q_{nom} is the rated capacity of the battery. The general expression C/hh indicates that the number of hours to completely discharge the battery at a constant current is hh.[38]

Table I. Lithium-ion battery parameters for both electrode and electrolyte phases as reported in Refs. 45–51. Values of k reported in Refs. 45–51 have been appropriately normalized by F and c_{max} such that the dimensions of k are consistent with (2).

Electrode	ℓ [m]	L [m]	ε [-]	k [A · m · mol^{-1}]	c_{max} [mol · m^{-3}]	D^e [m^{2}sec^{-1}]	K^e [Ω^{-1}m^{-1}]	D^s [m^{2}sec^{-1}]	K^s [Ω^{-1}m^{-1}]	Ref.
LiC_6	1.02e-6	9.85e-5	1.04e-2	6.15e-4	26000	3.94e-11	0.192	9.89e-14	100	45
LiC_6	2.5e-5	1.62e-4	0.154	7.5e-4	28200	2.93e-10	1.29	1e-13	100	46
LiC_6	2e-6	7.9e-5	0.025	3.02e-4	31540	2.3e-10	1.323	3.9e-14	2	47
Li_xC_6	2e-5	1.13e-4	0.177	3.11e-4	26000	2.6e-10	1	3.9e-14	100	48
$Li_{1-x}C_6$	2e-6	3.7e-5	0.054	1.75e-2	16,100	2.6e-10	5.676	2e-16	100	49
$LiCoO_2$	2e-5	1.05e-4	0.190	4.36e-4	51000	2.6e-10	1	1e-13	100	48
$LiFePO_4$	3.31e-8	9.5e-5	3.48e-4	1.15e-4	22806	3.94e-11	0.192	4.29e-18	0.49	45
$LiFePO_4$	2e-6	1.12e-4	0.152	5.68e-4	26390	2.3e-10	1.323	1.25e-15	0.01	47
$Li_4Ti_5O_{12}$	1.075e-8	9.6e-5	1.12e-4	1.49e7	51385	2e-10	0.38	6.8e-15	100	50,51
$LiNi_{1/3}Mn_{1/3}Co_{1/3}O_2$	2.4e-6	8.6e-5	0.028	9.92e-3	51385	2e-10	0.38	2.5e-16	139	50,51
$LiNi_{0.8}Co_{0.2-x}Al_xO_2$	8e-6	8.6e-5	0.093	5.5e-3	49195	2.93e-10	1.29	2e-13	10	46
$Li_xNi_yCo_zAl_{1-y-z}O_2$	2.5e-6	2.9e-5	0.086	9.76e-3	23,900	2.6e-1	5.676	3.7e-16	10	49

Table II. Dimensionless transport parameters calculated from (7) and (19) for the battery chemistry listed in Table I.

Electrode	Da_e [-]	Pe_e [-]	α [-]	β [-]	Da_s [-]	Pe_s [-]	δ [-]	γ [-]	Ref.
LiC_6	1.59e-2	4.98e-2	−0.66	0.91	6.35	1.03e4	2.02	−0.40	45
LiC_6	4.3e-3	4.16e-2	−1.70	2.92	1.26e1	9.44e3	4.90	−1.36	46
LiC_6	1.08e-3	4.85e-2	−0.82	1.86	6.35	4.33e2	1.65	−0.50	47
Li_xC_6	1.4e-3	3.94e-2	−1.87	3.79	9.34	2.62e4	5.88	−1.29	48
$Li_{1-x}C_6$	2.58e-2	3.61e-1	−0.35	1.25	3.36e4	8.27e6	5.46	−3.57	49
$LiCoO_2$	1.82e-3	2.01e-2	−2.36	3.80	4.74	5.22e3	5.16	−0.94	48
$LiFePO_4$	2.87e-3	5.68e-2	−0.36	0.74	2.64e4	1.33e6	1.77	−1.28	45
$LiFePO_4$	2.87e-3	5.8e-2	−0.71	1.45	5.28e2	8.07e1	1.09	−1.56	47
$Li_4Ti_5O_{12}$	7.4e7	9.84e-3	−0.51	−1.99	2.18e12	7.62e4	1.24	−3.12	50,51
$LiNi_{1/3}Mn_{1/3}Co_{1/3}O_2$	4.42e-2	9.84e-3	−1.29	0.87	3.54e4	2.88e6	4.16	−2.93	50,51
$LiNi_{0.8}Co_{0.2-x}Al_xO_2$	1.67e-2	2.38e-2	−1.57	1.72	2.45e1	2.70e2	2.36	−1.35	46
$Li_xNi_yCo_zAl_{1-y-z}O_2$	1.13e-2	2.43e-1	−0.58	1.83	7.93e3	3.01e5	5.15	−3.66	49

of the most popular models on which Partial Differential Equation (PDE) control and estimation strategies are based upon are, e.g., Newman's model,[8] its generalizations[43] and the single particle model (SPM).[44] Such models have the advantage of being relatively simple for controller/observer design as they are classical macroscopic/upscaled models which treat the complex porous structure and the electrolyte as superimposed fully-connected continua.

For example, the SPM is based on the key idea that the solid phase of each electrode can be idealized as a single spherical particle, while the electrolyte lithium-ion concentration is constant in space and time.[44] Its governing equations therefore reduce to Fick's law in spherical coordinates and can be readily derived from (20)-(21) and (26)-(27) under the appropriate model assumptions (e.g. constant $\langle c_e \rangle_{\mathcal{B}}$ and negligible electromigration). Similarly, Newman's model[8] can be obtained from (20)-(21) and (26)-(27) by relaxing the assumption that $\langle c_e \rangle_{\mathcal{B}}$ is approximately constant and including the full mass transport equation in the electrolyte phase (20), while still assuming negligible electromigration.

As such, these models are based on the fundamental, and often untested, assumption that separation of scales occurs and, consequently, macroscopic representations of averaged quantities can describe pore-scale processes with an accuracy prescribed by mathematical homogenization. Yet, since their validity is limited to the same constraints identified in Figures 1 and 2, they should be used with caution when the sufficient conditions listed above are violated. In the following section, we demonstrate the use of the phase diagrams in Figures 1 and 2 to a priori estimate macroscale models accuracy compared to their fully resolved counterparts for commercial battery systems.

Case Study for Commercial Batteries: Validity of Macroscale Models

In this section, we investigate the validity of macroscale models in relations to: 1) different chemistry, and 2) different conditions of operation in terms of temperature and C-rate for a series of commercially available batteries. In particular, we compare the accuracy of continuum-scale models with either their fully resolved (3D) counterparts or with experiments as reported in a number of studies.[45–51] More importantly, we relate macroscale models' predictive performance to the applicability regimes defined in Figures (1) and (2), and employ the former as a screening tool to a priori evaluate continuum model predictivity under variable C-rate.

Chemistry dependence of macroscale models.— The battery cell parameter data used in this case study, and reported in Table I, are based on a variety of electrode and electrolyte compositions at room temperature ($T = 298$ K).[45–51] The dimensionless parameters α, β, γ and δ in the electrolyte and electrode phases, readily calculated from (7) and (19), are reported in Table II and plotted on the corresponding phase diagram for the electrolyte and electrode, Figure 3 and 4, respectively.

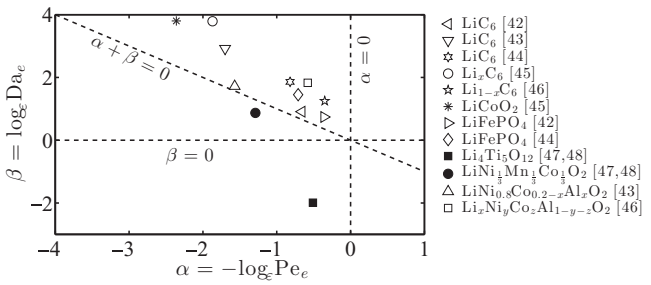

Figure 3. Values of the dimensionless parameters for the most commonly used lithium-ion battery materials. These values, determined at room temperature (298 K), lie either inside the electrolyte applicability regime region (empty symbols) or outside (filled symbols).

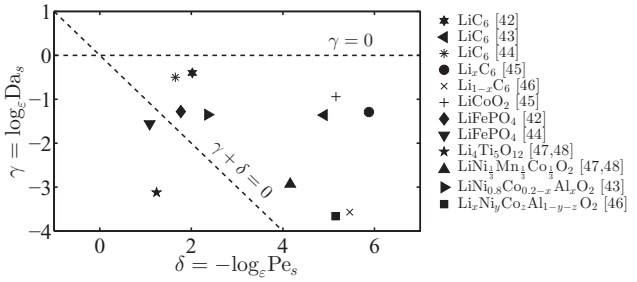

Figure 4. Values of the dimensionless parameters (δ, γ) for the most commonly used lithium-ion battery materials. These values, determined at room temperature (298 K), all lie outside the electrode applicability regime region.

Among the twelve chemistry considered in this analysis,[45–51] ten possess electrolyte effective transport coefficients, i.e. dimensionless numbers (α, β), which do not violate the applicability conditions of macroscale models, see Figure 3. The theory developed previously ensures that the homogenized equations in the electrolyte will be able to accurately capture the dynamics at the pore-scale: this is consistent with the numerical simulations performed in Refs. 45–51, where Newman-type models have been successfully used to model transport in the electrolyte phase. On the contrary, two data points (solid symbols in Figure 3), corresponding to $Li_4Ti_5O_{12}$ and $LiNi_{1/3}Mn_{1/3}Co_{1/3}O_2$ chemistry,[50,51] lie outside the range of applicability. For these two chemistry, it is not guaranteed that the homogenized Equations (20) and (21) describing transport in the electrolyte will be effective in capturing pore-scale transport processes. Again, this is confirmed by the results presented in Refs. 50, 51, where a Newman-type model response could not properly capture experimental data, see Fig. 6 in Ref. 51. Such a discrepancy is understandable: $Li_4Ti_5O_{12}$ has a very fast intercalation reaction rate (between 6 and 9 orders of magnitude faster than the other chemistry) which leads to mass transport limitations (or reaction-dominated regimes) and lack of pore-scale mixing.

Figure 4 shows the data points corresponding to the (δ, γ) values for the battery chemistry electrodes listed in Table I and calculated in Table II. All the data points lie outside the range of applicability of the upscaled equations of lithium-ion transport in the electrode phase, therefore suggesting that full pore-scale models have to be employed to accurately capture lithium-ion transport in the active particles. This is consistent with the numerical approaches used in Refs. 45–51, where no upscaled model is used in the active particles and the transport in the solid electrode is solved at the microscale. It is worth noticing that, since bounds on α, β, γ and δ have to be *concurrently* satisfied, the numerical simulations matched well the experiments only when the conditions on (α, β) were not violated, as discussed previously.

Operating conditions' dependence of macroscale models.— Figures 3 and 4 showed the distribution of the dimensionless transport parameters α, β, γ and δ at room temperature in the phase diagrams and allowed one to a priori assess the validity of Newman-type models across different battery chemistry. These models, on the other hand, might also fail when used for the *proper chemistry* (i.e., the chemistry for which the corresponding α and β data points fall in the applicability regime regions at room temperature) but *improper operating conditions*. For this reason, the veracity of the upscaled equations of mass and charge transport in the electrolyte across battery cell operating conditions is also investigated. In particular, the study conducted in this section focuses on temperature and C-rate of operation and uses the electrode-electrolyte system described in Ref. 52. In this work, the authors compared the performance of their (continuum-scale) numerical simulations with experimental data for lithium-ion cells with $Li_yMn_2O_4$ and $LiNi_{0.8}Co_{0.15}Al_{0.05}O_2$ cathode materials tested at different C-rate ranging from C/25 to 10C. We conduct our analysis for the case of $Li_yMn_2O_4$ cathode material, but similar results can be easily extended to the $LiNi_{0.8}Co_{0.15}Al_{0.05}O_2$ case.

Table III. Reference reaction rate constants k_{ref} for lithium manganate cathode in terms of applied current I_{app}.

C-rate [1/h]	I_{app} [A/m^2]	k_{ref} [A · m · mol^{-1}]
C/25	0.34	2.03e-5
1C	8.5	5.07e-4
10C	85	5.07e-3

The case study analysis relies on the premise that temperature is one of the primary factors that influences the ability of the macroscale transport equations to capture battery dynamics at high C-rate. In fact, the battery cell temperature influences the transport parameters in the electrolyte phase. Those parameters are: k (reaction rate constant), D^e (the electrolyte diffusion coefficient), and K^e (the electrolyte conductivity coefficient). When the influence of temperature on k is much more pronounced than on D^e and K^e, as we will verify in the case of a battery operating at high C-rate, diffusion is no longer the dominant mode of transport. In this case the homogenized transport equations do not accurately capture transport at the microscale.

A single and constant value for the reaction rate k was considered in Ref. 52. Yet, experimental evidence shows significant cell temperature variations in terms of C-rate.[53–58] Our analysis is conducted for three different C-rate: low (C/25), medium (1C), and high (10C). Following experimental data,[53–58] the temperature increase, starting from room tenperature, can be estimated as follows: from 298 K to 299 K, from 298 K to 306 K, and from 298 K to 333 K at a discharge C-rate of C/25, 1C and 10C, respectively. We estimate the reaction rate constant k_{ref} at room temperature T_{ref} =298 K through

$$I_{app} = 2 \cdot k_{ref} \cdot \sqrt{\hat{c}^e_\varepsilon \hat{c}^s_\varepsilon \left(1 - \frac{\hat{c}^s_\varepsilon}{\hat{c}^s_{\max}}\right)} \cdot \sinh[F(\hat{\phi}^s_\varepsilon - \hat{\phi}^e_\varepsilon - \hat{U})/2RT_{ref}] \quad [30]$$

where I_{app} (A/m^2), the applied current density, is provided in Ref. 59 for each C-rate, see Table III. The electrochemical reaction rate constant $k(T)$ for a given electrode system can be described as a function of temperature using the Arrhenius equation, as reported in Ref. 60:

$$k(T) = k_{ref} \exp\left[\frac{Ea_r}{R}\left(\frac{1}{T_{ref}} - \frac{1}{T}\right)\right], \quad [31]$$

where $k(T)$ is the reaction rate constant of a given electrode at the desired temperature T. In (31), Ea_r is the electrode reaction rate activation energy. We set Ea_r = 78.24 kJ/mol at a reference temperature of 298 K.[61] Using (31), we compute the values of k for different temperature conditions, which are then used to determine the parameter values α and β.

Similarly, the diffusion and conductivity coefficients, D^e and K^e, vary as a function of both temperature and the lithium concentration in the electrolyte phase. For the estimate of D^e and K^e at the reference temperature T_{ref}, we use the same approach used in Ref. 52, where:

$$D^e = 6.5 \cdot 10^{-10} \exp\left(-0.7\frac{\hat{c}^e_\varepsilon}{1000}\right), \quad [32]$$

$$K^e = 0.84\left(\frac{1.134(\hat{c}^e_\varepsilon/1000)}{1 + 0.2(\hat{c}^e_\varepsilon/1000) + 0.08(\hat{c}^e_\varepsilon/1000)^4} + 0.1\right), \quad [33]$$

where we set $\hat{c}^e_\varepsilon$ = 1500 mol/m^3 ([d]). This leads to reference values of 2.41e-10 m^2/s and 0.922 S/m for D^e and K^e, respectively. Since, to the best of our knowledge, no analytical dependence on temperature is available for D^e and K^e, we use instead a curve fitting procedure from

[d]From Ref. 52, $\hat{c}^e_\varepsilon$ varies in the range of 1,000 to 2,000 mol/m^3 over the entire duration of the simulations.

Table IV. Dimensionless transport parameters of $Li_yMn_2O_4$ cathode for different C-rate and temperatures.

C-rate [1/h]	ℓ [m]	L [m]	ε [-]	k [A · m · mol^{-1}]	T [K]	D^e [m^{2}sec^{-1}]	K^e [Ω^{-1}m^{-1}]	Da$_e$ [-]	Pe$_e$ [-]	α [-]	β [-]
C/25	3.4e-6	1e-4	0.034	2.03e-5	298	2.41e-10	0.922	8.72e-5	4.26e-2	−0.93	2.76
C/25	3.4e-6	1e-4	0.034	2.07e-5	298.2	2.41e-10	0.922	8.91e-5	4.26e-2	−0.93	2.76
C/25	3.4e-6	1e-4	0.034	2.12e-5	298.4	2.41e-10	0.922	9.1e-5	4.27e-2	−0.93	2.75
C/25	3.4e-6	1e-4	0.034	2.16e-5	298.6	2.41e-10	0.922	9.29e-5	4.27e-2	−0.93	2.75
C/25	3.4e-6	1e-4	0.034	2.25e-5	299.0	2.41e-10	0.922	9.69e-5	4.27e-2	−0.93	2.73
1C	3.4e-6	1e-4	0.034	5.07e-4	298	2.41e-10	0.922	2.18e-3	4.26e-2	−0.93	1.81
1C	3.4e-6	1e-4	0.034	6.26e-4	300	2.55e-10	0.972	2.55e-3	4.28e-2	−0.93	1.77
1C	3.4e-6	1e-4	0.034	7.70e-4	302	2.69e-10	1.022	2.97e-3	4.29e-2	−0.93	1.72
1C	3.4e-6	1e-4	0.034	9.45e-4	304	2.82e-10	1.072	3.47e-3	4.31e-2	−0.93	1.67
1C	3.4e-6	1e-4	0.034	1.16e-3	306	2.96e-10	1.122	4.05e-3	4.33e-2	−0.93	1.63
10C	3.4e-6	1e-4	0.034	5.07e-3	298	2.41e-10	0.922	2.18e-2	4.26e-2	−0.93	1.13
10C	3.4e-6	1e-4	0.034	8.54e-3	303	2.75e-10	1.047	3.21e-2	4.30e-2	−0.93	1.02
10C	3.4e-6	1e-4	0.034	2.30e-2	313	3.44e-10	1.297	6.93e-2	4.41e-2	−0.92	0.79
10C	3.4e-6	1e-4	0.034	5.84e-2	323	4.13e-10	1.547	1.47e-1	4.52e-2	−0.92	0.57
10C	3.4e-6	1e-4	0.034	1.40e-1	333	4.82e-10	1.797	3.01e-1	4.64e-2	−0.91	0.35

Figures 13 and 14 in Ref. 62 to determine $D^e(T)$ and $K^e(T)$. A summary of the estimated parameters for different C-rate and temperature ranges is given in Table IV.

Based on above calculations, we determine the temperature-dependent trajectories of the data points (α,β) computed at the temperature intervals characteristic of each C-rate. Table IV summarizes the variation of parameters α and β as a function of the operating conditions for the three C-rate of interest. The data points and their variation with temperature and C-rate are schematically represented in Figure 5.

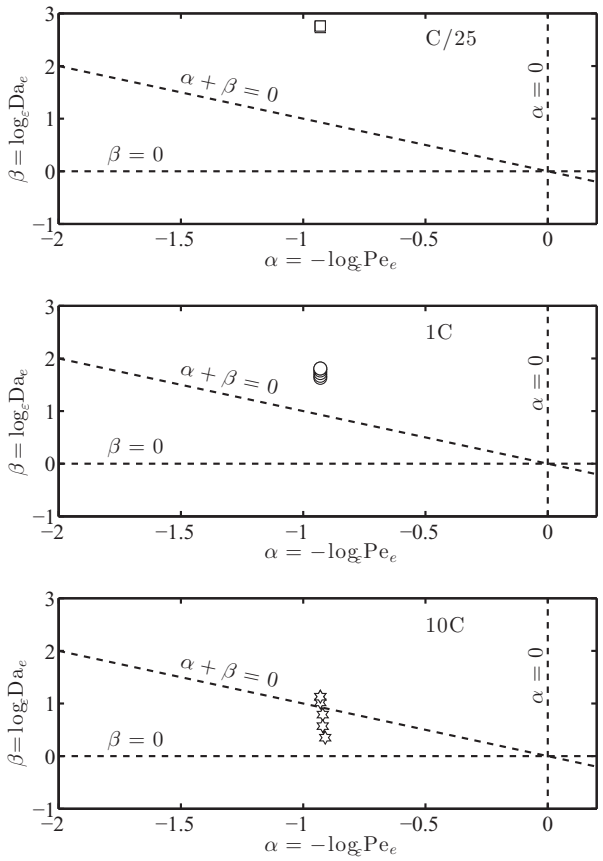

Figure 5. Variation with temperature of dimensionless parameters α and β in lithium manganate cathode batteries for three different C-rate of discharge, C/25 (top), 1C (middle) and 10C (bottom). An increase in C-rate induces higher operating temperature variations inside a battery: as a result the system can be driven outside the applicability regime region.

Figure 5 (top) shows that at a C/25 rate of discharge, there is minimal temperature increase over the duration of a discharge event. The magnitude of parameter α remains invariant, while β increases slightly due to an increase in the Da$_e$ number. The behavior of the system (as a function of temperature) is linear with β. The data points satisfy the constraints on α and β. Hence, the upscaled equations for lithium mass transport should provide an accurate description of the pore scale behavior. This is consistent with the simulation results from a continuum-scale simulator obtained in Figure 7(a) of Ref. 52, where there is a perfect match between the model and the experimental response.

At a 1C rate of discharge, Figure 4 (middle), there is a moderate increase in temperature over the duration of the simulation cycle. The magnitude of parameter α remains invariant, while β increases at a moderate rate due to a faster increase in the Da$_e$ number. The behavior of this system is linear in α and β. At elevated temperatures, the effect of increase in the reaction rate constant k dominates any increase of D^e and K^e. The data points satisfy the constraints on α and β over the range of operating temperature conditions. Hence the homogenized set of transport equations used in Ref. 52, Figure 7(a), still provides an accurate description of the pore scale behavior, leading to good correlation with experimental data.

At a 10C rate of discharge, there is a very significant increase in the battery temperature over the operating conditions. There is a very small increase in α as the increase in D^e marginally dominates the increase in K^e, leading to an incremental increase in the Pe$_e$ number. The reaction rate constant is 2 to 3 orders of magnitude higher than at lower C-rate; hence, the rate of decrease in β is higher than the rate of increase in α. For the $LiMn_2O_4$ cathode system, the macroscale transport equations are no longer accurate in describing microscale transport processes at temperatures 313 K or higher. This is because the value of α + β is less than 0, which violates one of the three constraints on these two parameters. At high operating temperatures and C-rate, the lithium manganate cathode system operates in a transport regime where the three lithium transport processes (reaction, diffusion, and electro-migration) are of the same order. In this scenario, very fast reaction kinetics lead to diffusion-limited regimes where diffusion is no longer the dominant transport mechanism in the medium. As a result, macroscale equations describing electrolyte transport are vulnerable and can be invalidated due to lack of scale separation with respect to the pore-scale.

The performance prediction of continuum-scale models based on the phase diagram Figure 4 (bottom) is, again, consistent with the analysis performed in Ref. 52, Figure 7(a), where the numerical solution obtained from macroscopic models cannot capture the experimental results. Under these circumstances, a multi-scale model is necessary to incorporate the effects of transport both at the pore-scale and the macroscopic scale.

The approach implemented above is significant in terms of identifying the temperature of operation and C-rate of current charge/discharge as crucial parameters dictating the dominance of one transport mechanism over the other(s) in the battery electrode/electrolyte medium. Standard Newman-type macroscopic models under scenarios similar to the one described above are invalid and may fail to capture microscale transport processes.

Conclusions

Lithium-ion transport in batteries involves diffusion, electromigration and heterogeneous intercalation reactions occurring in geometrically complex porous electrodes. As such, ion transport can be modeled on a multiplicity of scales, ranging from the pore- to the system-scale. Macroscopic models, which are approximate representations of the pore-scale physics, are advantageous due to their simplicity (relative to fully pore-scale descriptions) and their limited computational burden. These two aspects render them particularly appealing for PDE-based control and estimation strategies of SOH and SOC. Yet, macroscale models are known to fail as predictive tools under given operating conditions, e.g. high C-rate and high temperature. This hampers any control and design strategies based on them.

In this work we establish the robustness of macroscopic diffusion-migration-reaction (DRM) equations that describe the evolution of mean (spatially averaged) lithium-ion concentration and potential in the electrolyte and electrode phases, treated as overlapping continua. Starting from the equations describing lithium-ion transport at the pore-scale, we use multiple scale expansions to rigorously derive macroscopic dual-continua models and identify under which conditions they describe micro-scale dynamics with the accuracy prescribed by the homogenization technique. The relative importance between diffusion, conduction, and reaction can be quantified by electric Péclet Pe_j and Damköhler Da_j, $j = \{e, s\}$, numbers in the electrolyte and electrode phases.

Our main result, summarized in the two (Da,Pe)-phase diagrams, is the identification of the sufficient conditions needed to guarantee that the pore- and the continuum-scales can be separated and the system of macroscopic diffusion-reaction-migration Equations (20)-(21) and (26)-(27) accurately represents pore scale processes. Such conditions are expressed in terms of bounds on the order of magnitude of Pe_j and Da_j, $j = \{e, s\}$ and indicate that there may be entire classes of battery chemistry for which macroscopic models are not accurate descriptors of micro-scale dynamics.

We showed the distribution of parameters Pe_j and Da_j in the electrolyte and electrode phase diagrams for different chemical compositions of the most common commercial batteries, for which the transport parameters have been experimentally determined or estimated based on analytical techniques for the purpose of numerical simulations. More importantly, we validated the new conditions over a case study, where we have determined the transport parameters Pe_e and Da_e (or α and β) in the electrolyte phase diagram for different operating conditions based on battery chemistry composition, temperature and C-rate. The performance predictions of continuum models based on a phase diagram analysis confirmed the results independenently obtained from other numerical and experimental studies, i.e. a breakdown of continuum models at high C-rate.

Bounds on parameters Pe_j and Da_j, $j = \{e, s\}$ also highlight the importance of mixing at the sub-pore scale for continuum equations to be valid. In this regard, diffusion-limited regimes due to either fast reaction kinetics (e.g. at high operating temperatures) and/or fast electromigration are the critical scenarios where separation of scales may lack and continuum models be invalidated. Models that account for a full coupling between the two scales must be employed instead,[63] and replace classical continuum models (e.g. single particle models) if accurate predictions of the battery response under different operating conditions are sought.

To the best of our knowledge, the literature lacks in such a systematic method to guide researchers in the use of the correct modeling tools for battery systems. Future SOH and SOC estimations based on macroscopic models should account for model robustness and error, whenever scale separation cannot be guaranteed, e.g., at high C-rate.

Appendix A: Homogenization in the Electrolyte

We set $c_\varepsilon^j(\mathbf{x}, t) = c^j(\mathbf{x}, \mathbf{y}, t, \tau_\mathrm{r}, \tau_{\mathrm{me}}, \tau_{\mathrm{ms}})$ and $\phi_\varepsilon^j(\mathbf{x}, t) = \phi^j(\mathbf{x}, \mathbf{y}, t, \tau_\mathrm{r}, \tau_{\mathrm{me}}, \tau_{\mathrm{ms}})$, $j = \{e, s\}$. Then, combining (17) with (8a) and (8b) we obtain

$$\frac{\partial c^e}{\partial t} + \mathrm{Da}_e \frac{\partial c^e}{\partial \tau_\mathrm{r}} + \mathrm{Pe}_e \left(\frac{\partial c^e}{\partial \tau_{\mathrm{me}}} + \frac{\mathrm{Da}_e}{\mathrm{Da}_s} \frac{\partial c^e}{\partial \tau_{\mathrm{ms}}} \right)$$
$$= \nabla_\mathbf{x} \cdot [(\mathbf{D}^e + \lambda t_+^2 \mathrm{Pe}_e \mathbf{K}^e / c^e)(\nabla_\mathbf{x} c^e + \varepsilon^{-1} \nabla_\mathbf{y} c^e) + 2 t_+ \mathrm{Pe}_e \mathbf{K}^e (\nabla_\mathbf{x} \phi^e + \varepsilon^{-1} \nabla_\mathbf{y} \phi^e)]$$
$$+ \varepsilon^{-1} \nabla_\mathbf{y} \cdot [(\mathbf{D}^e + \lambda t_+^2 \mathrm{Pe}_e \mathbf{K}^e / c^e)(\nabla_\mathbf{x} c^e + \varepsilon^{-1} \nabla_\mathbf{y} c^e) + 2 t_+ \mathrm{Pe}_e \mathbf{K}^e (\nabla_\mathbf{x} \phi^e + \varepsilon^{-1} \nabla_\mathbf{y} \phi^e)] \quad [A1]$$

and

$$\nabla_\mathbf{x} \cdot [(\lambda t_+ \mathrm{Pe}_e \mathbf{K}^e / c_e)(\nabla_\mathbf{x} c^e + \varepsilon^{-1} \nabla_\mathbf{y} c^e) + 2 \mathbf{K}^e \mathrm{Pe}_e (\nabla_\mathbf{x} \phi^e + \varepsilon^{-1} \nabla_\mathbf{y} \phi^e)]$$
$$+ \varepsilon^{-1} \nabla_\mathbf{y} \cdot [\mathbf{K}^e (\lambda t_+ \mathrm{Pe}_e / c^e)(\nabla_\mathbf{x} c^e + \varepsilon^{-1} \nabla_\mathbf{y} c^e) + 2 \mathbf{K}^e \mathrm{Pe}_e (\nabla_\mathbf{x} \phi^e + \varepsilon^{-1} \nabla_\mathbf{y} \phi^e)] = 0, \quad [A2]$$

for $\mathbf{y} \in \mathcal{B}$, subject to

$$\mathbf{n}_e \cdot [(\mathbf{D}^e + \lambda t_+^2 \mathrm{Pe}_e \mathbf{K}^e / c^e)(\nabla_\mathbf{x} c^e + \varepsilon^{-1} \nabla_\mathbf{y} c^e) + 2 t_+ \mathrm{Pe}_e \mathbf{K}^e (\nabla_\mathbf{x} \phi^e + \varepsilon^{-1} \nabla_\mathbf{y} \phi^e)]$$
$$= \mathrm{Da}_e f(c_\varepsilon^e, c_\varepsilon^s, \phi_\varepsilon^s, \phi_\varepsilon^e) \quad \mathbf{y} \in \Gamma, \quad [A3]$$

and

$$\mathbf{n}_e \cdot [(\lambda t_+ \mathrm{Pe}_e \mathbf{K}^e / c^e)(\nabla_\mathbf{x} c^e + \varepsilon^{-1} \nabla_\mathbf{y} c^e) + 2 \mathrm{Pe}_e \mathbf{K}^e (\nabla_\mathbf{x} \phi^e + \varepsilon^{-1} \nabla_\mathbf{y} \phi^e)]$$
$$= \mathrm{Da}_e f(c_\varepsilon^e, c_\varepsilon^s, \phi_\varepsilon^s, \phi_\varepsilon^e), \qquad \mathbf{y} \in \Gamma, \quad [A4]$$

respectively, where $f(c_\varepsilon^e, c_\varepsilon^s, \phi_\varepsilon^s, \phi_\varepsilon^e)$ is defined in (10).

Mass and charge transport asymptotic expansions.— Substituting (18) and (19) into the mass transport equation in the electrolyte (8) leads to

$$\varepsilon^{-2}\{-\nabla_\mathbf{y} \cdot [(\mathbf{D}^e + \varepsilon^{-\alpha} \lambda t_+^2 \mathbf{K}^e / c_0^e) \nabla_\mathbf{y} c_0^e + 2\varepsilon^{-\alpha} t_+ \mathbf{K}^e \nabla_\mathbf{y} \phi_0^e)]\}$$
$$+ \varepsilon^{-1}\{\varepsilon^{1+\beta} \partial_{\tau_\mathrm{r}} c_0^e - \nabla_\mathbf{x} \cdot [(\mathbf{D}^e + \varepsilon^{-\alpha} \lambda t_+^2 \mathbf{K}^e / c_0^e) \nabla_\mathbf{y} c_0^e + 2\varepsilon^{-\alpha} t_+ \mathbf{K}^e \nabla_\mathbf{y} \phi_0^e]$$
$$- \nabla_\mathbf{y} \cdot [(\mathbf{D}^e + \varepsilon^{-\alpha} \lambda t_+^2 \mathbf{K}^e / c_0^e)(\nabla_\mathbf{x} c_0^e + \nabla_\mathbf{y} c_1^e) + \varepsilon^{-\alpha} \lambda t_+^2 \mathbf{K}^e (c_1^e / c_0^e) / c_0^e \nabla_\mathbf{y} c_0^e$$
$$+ 2\varepsilon^{-\alpha} t_+ \mathbf{K}^e (\nabla_\mathbf{x} \phi_0^e + \nabla_\mathbf{y} \phi_1^e)]\}$$
$$+ \varepsilon^0\{\partial_t c_0^e + \varepsilon^{-\alpha}(\partial_{\tau_{\mathrm{me}}} c_0^e + \varepsilon^{\beta-\gamma} \partial_{\tau_{\mathrm{ms}}} c_0^e) + \varepsilon^{1+\beta} \partial_{\tau_\mathrm{r}} c_1^e$$
$$- \nabla_\mathbf{x} \cdot [(\mathbf{D}^e + \varepsilon^{-\alpha} \lambda t_+^2 \mathbf{K}^e / c_0^e)(\nabla_\mathbf{x} c_0^e + \nabla_\mathbf{y} c_1^e) + \varepsilon^{-\alpha} \lambda t_+^2 \mathbf{K}^e (c_1^e / c_0^e) / c_0^e \nabla_\mathbf{y} c_0^e$$
$$+ 2\varepsilon^{-\alpha} t_+ \mathbf{K}^e (\nabla_\mathbf{x} \phi_0^e + \nabla_\mathbf{y} \phi_1^e)] - \nabla_\mathbf{y} \cdot [(\mathbf{D}^e + \varepsilon^{-\alpha} \lambda t_+^2 \mathbf{K}^e / c_0^e)(\nabla_\mathbf{x} c_1^e + \nabla_\mathbf{y} c_2^e)$$
$$- \varepsilon^{-\alpha} \lambda t_+^2 \mathbf{K}^e (c_1^e / c_0^e) / c_0^e (\nabla_\mathbf{x} c_0^e + \nabla_\mathbf{y} c_1^e) + \varepsilon^{-\alpha} \lambda t_+^2 \mathbf{K}^e / c_0^e [(c_1^e / c_0^e)^2 - c_2^e / c_0^e] \nabla_\mathbf{y} c_0^e$$
$$+ 2\varepsilon^{-\alpha} t_+ \mathbf{K}^e (\nabla_\mathbf{x} \phi_1^e + \nabla_\mathbf{y} \phi_2^e)]\} = \mathcal{O}(\varepsilon), \qquad \mathbf{y} \in \mathcal{B}, \quad [A5]$$

where the nonlinear term in (8) is expanded in a Mclaurin series

$$1/c^e \approx (c_0 + \varepsilon c_1^e + \varepsilon^2 c_2^e)^{-1} \approx \frac{1}{c_0} \left\{ 1 - \varepsilon \frac{c_1^e}{c_0^e} + \varepsilon^2 \left[\left(\frac{c_1^e}{c_0^e} \right)^2 - \left(\frac{c_2^e}{c_0^e} \right) \right] \right\}. \quad [A6]$$

Similarly, the interface condition (A3) can be written as

$$\varepsilon^{-1}\{\mathbf{n}_e \cdot [(\mathbf{D}^e + \varepsilon^{-\alpha} \lambda t_+^2 \mathbf{K}^e / c_0^e) \nabla_\mathbf{y} c_0^e + 2\varepsilon^{-\alpha} t_+ \mathbf{K}^e \nabla_\mathbf{y} \phi_0^e]\}$$
$$+ \varepsilon^0\{\mathbf{n}_e \cdot [(\mathbf{D}^e + \varepsilon^{-\alpha} \lambda t_+^2 \mathbf{K}^e / c_0^e)(\nabla_\mathbf{x} c_0^e + \nabla_\mathbf{y} c_1^e) - \varepsilon^{-\alpha} \lambda t_+^2 \mathbf{K}^e / c_0^e (c_1^e / c_0^e) \nabla_\mathbf{y} c_0^e)$$
$$+ 2\varepsilon^{-\alpha} t_+ \mathbf{K}^e (\nabla_\mathbf{x} \phi_0^e + \nabla_\mathbf{y} \phi_1^e)] - 2\varepsilon^\beta A_0 B_0)\}$$
$$+ \varepsilon\{\mathbf{n}_e \cdot [(\mathbf{D}^e + \varepsilon^{-\alpha} \lambda t_+^2 \mathbf{K}^e / c_0^e)(\nabla_\mathbf{x} c_1^e + \nabla_\mathbf{y} c_2^e) + 2\varepsilon^{-\alpha} t_+ \mathbf{K}^e (\nabla_\mathbf{x} \phi_1^e + \nabla_\mathbf{y} \phi_2^e)$$
$$- \varepsilon^{-\alpha} \lambda t_+^2 \mathbf{K}^e / c_0^e (c_1^e / c_0^e)(\nabla_\mathbf{x} c_0^e + \nabla_\mathbf{y} c_1^e) + \varepsilon^{-\alpha} \lambda t_+^2 \mathbf{K}^e / c_0^e [(c_1^e / c_0^e)^2 - (c_2 / c_0)] \nabla_\mathbf{y} c_0^e$$
$$- 2\varepsilon^\beta (A_0 B_1 + A_1 B_0)]\} = \mathcal{O}(\varepsilon^2), \quad \mathbf{y} \in \Gamma, \quad [A7]$$

since $\sinh(\phi^s - \phi^e - U) = \sinh(\phi_0^s - \phi_0^e - U) + \varepsilon(\phi_1^s - \phi_1^e)\cosh(\phi_0^s - \phi_0^e - U) + \mathcal{O}(\varepsilon^2)$, where

$$A_0 = \sinh(\phi_0^s - \phi_0^e - U), \quad [A8a]$$

$$B_0 = \sqrt{c_0^e c_0^s (1 - c_0^s)}, \quad [A8b]$$

$$A_1 = (\phi_1^s - \phi_1^e)\cosh(\phi_0^s - \phi_0^e - U), \quad [A8c]$$

$$B_1 = \sqrt{c_0^e c_0^s (1 - c_0^s)} \left[\frac{c_1^s}{2 c_0^s} + \frac{c_1^e}{2 c_0^e} - \frac{c_1^s}{2(1 - c_0^s)} \right]. \quad [A8d]$$

Combining (18) and (19) with the charge transport Equation (A2) and boundary condition (A4) yields to

$$\begin{aligned}
&\varepsilon^{-2}\{\nabla_{\mathbf{y}}\cdot[\lambda t_+\mathbf{K}^e/c_0^e\nabla_{\mathbf{y}}c_0^e+2\mathbf{K}^e\nabla_{\mathbf{y}}\phi_0^e]\}\\
&+\varepsilon^{-1}\{\nabla_{\mathbf{x}}\cdot[\lambda t_+\mathbf{K}^e/c_0^e\nabla_{\mathbf{y}}c_0^e+2\mathbf{K}^e\nabla_{\mathbf{y}}\phi_0^e]+\nabla_{\mathbf{y}}\cdot[\lambda t_+\mathbf{K}^e/c_0^e(\nabla_{\mathbf{x}}c_0^e+\nabla_{\mathbf{y}}c_1^e)\\
&-\lambda t_+\mathbf{K}^e(c_1^e/c_0^e)/c_0^e\nabla_{\mathbf{y}}c_0^e+2\mathbf{K}^e(\nabla_{\mathbf{x}}\phi_0^e+\nabla_{\mathbf{y}}\phi_1^e)]\}\\
&+\varepsilon^{0}\{\nabla_{\mathbf{x}}\cdot[\lambda t_+\mathbf{K}^e/c_0^e(\nabla_{\mathbf{x}}c_0^e+\nabla_{\mathbf{y}}c_1^e)-\lambda t_+\mathbf{K}^e(c_1^e/c_0^e)/c_0^e\nabla_{\mathbf{y}}c_0^e+2\mathbf{K}^e(\nabla_{\mathbf{x}}\phi_0^e+\nabla_{\mathbf{y}}\phi_1^e)\\
&+\nabla_{\mathbf{y}}\cdot[\lambda t_+\mathbf{K}^e/c_0^e(\nabla_{\mathbf{x}}c_1^e+\nabla_{\mathbf{y}}c_2^e)-\lambda t_+\mathbf{K}^e(c_1^e/c_0^e)/c_0^e(\nabla_{\mathbf{x}}c_0^e+\nabla_{\mathbf{y}}c_1^e)\\
&+\lambda t_+\mathbf{K}^e/c_0^e[(c_1^e/c_0^e)^2-c_2^e/c_0^e]\nabla_{\mathbf{y}}c_0^e+2\mathbf{K}^e(\nabla_{\mathbf{x}}\phi_1^e+\nabla_{\mathbf{y}}\phi_2^e)]\}=\mathcal{O}(\varepsilon),\quad \mathbf{y}\in\mathcal{B},
\end{aligned}\tag{A9}$$

subject to

$$\begin{aligned}
&\varepsilon^{-1}\{\mathbf{n}_e\cdot[\varepsilon^{-\alpha}\lambda t_+\mathbf{K}^e/c_0^e\nabla_{\mathbf{y}}c_0^e+2\varepsilon^{-\alpha}\mathbf{K}^e\nabla_{\mathbf{y}}\phi_0^e]\}\\
&+\varepsilon^{0}\{\mathbf{n}_e\cdot[\varepsilon^{-\alpha}\lambda t_+\mathbf{K}^e/c_0^e(\nabla_{\mathbf{x}}c_0^e+\nabla_{\mathbf{y}}c_1^e)-\varepsilon^{-\alpha}\lambda t_+\mathbf{K}^e/c_0^e(c_1^e/c_0^e)\nabla_{\mathbf{y}}c_0^e\\
&+2\varepsilon^{-\alpha}\mathbf{K}^e(\nabla_{\mathbf{x}}\phi_0^e+\nabla_{\mathbf{y}}\phi_1^e)-2\varepsilon^{\beta}A_0B_0]\}\\
&+\varepsilon\{\mathbf{n}_e\cdot[\varepsilon^{-\alpha}\lambda t_+\mathbf{K}^e/c_0^e(\nabla_{\mathbf{x}}c_1^e+\nabla_{\mathbf{y}}c_2^e)-\varepsilon^{-\alpha}\lambda t_+\mathbf{K}^e/c_0(c_1/c_0)(\nabla_{\mathbf{x}}c_0^e+\nabla_{\mathbf{y}}c_1^e)\\
&+\varepsilon^{-\alpha}\lambda t_+\mathbf{K}^e/c_0[(c_1^e/c_0^e)^2-c_2^e/c_0^e]\nabla_{\mathbf{y}}c_0^e+2\varepsilon^{-\alpha}\mathbf{K}^e(\nabla_{\mathbf{x}}\phi_1^e+\nabla_{\mathbf{y}}\phi_2^e)\\
&-2\varepsilon^{\beta}(A_0B_1+A_1B_0)\}=\mathcal{O}(\varepsilon^2),\quad \mathbf{y}\in\Gamma,
\end{aligned}\tag{A10}$$

where A_0, A_1, B_0 and B_1 are defined in (A8). Next, we compare terms of like-order of ε.

Terms of order $\mathcal{O}(\varepsilon^{-2})$.— Collecting the leading-order terms in the mass transport equation and corresponding boundary condition (A5) and (A7) respectively, we obtain

$$-\nabla_{\mathbf{y}}\cdot[(\mathbf{D}^e+\varepsilon^{-\alpha}\lambda t_+^2\mathbf{K}^e/c_0^e)\nabla_{\mathbf{y}}c_0^e+2\varepsilon^{-\alpha}t_+\mathbf{K}^e\nabla_{\mathbf{y}}\phi_0^e]=0,\quad \mathbf{y}\in\mathcal{B},\tag{A11}$$

subject to

$$\mathbf{n}_e\cdot[(\mathbf{D}^e+\varepsilon^{-\alpha}\lambda t_+^2\mathbf{K}^e/c_0^e)\nabla_{\mathbf{y}}c_0^e+2\varepsilon^{-\alpha}t_+\mathbf{K}^e\nabla_{\mathbf{y}}\phi_0^e)]=0,\quad \mathbf{y}\in\Gamma.\tag{A12}$$

Similarly, at the leading order the charge transport equation is

$$\nabla_{\mathbf{y}}\cdot(\lambda t_+\mathbf{K}^e/c_0^e\nabla_{\mathbf{y}}c_0^e+2\mathbf{K}^e\nabla_{\mathbf{y}}\phi_0^e)=0,\quad \mathbf{y}\in\mathcal{B},\tag{A13}$$

subject to

$$\mathbf{n}_e\cdot(\lambda t_+\mathbf{K}^e/c_0^e\nabla_{\mathbf{y}}c_0^e+2\mathbf{K}^e\nabla_{\mathbf{y}}\phi_0^e)=0,\quad \mathbf{y}\in\Gamma.\tag{A14}$$

Homogeneity of (A11)-(A12) and (A13)-(A14), guarantees that c_0^e and ϕ_0^e are independent of $\mathbf{y}$, i.e.

$$c_0^e=c_0^e(\mathbf{x},t,\tau_{\mathrm{r}},\tau_{me},\tau_{ms}),\tag{A15}$$

$$\phi_0^e=\phi_0^e(\mathbf{x},t,\tau_{\mathrm{r}},\tau_{me},\tau_{ms}).\tag{A16}$$

Terms of order $\mathcal{O}\left(\varepsilon^{-1}\right)$.— Since $\nabla_{\mathbf{y}}c_0^e\equiv\mathbf{0}$ and $\nabla_{\mathbf{y}}\phi_0^e\equiv\mathbf{0}$, the mass balance equation (A5) at order $\mathcal{O}(\varepsilon^{-1})$ simplifies to

$$\begin{aligned}
&\varepsilon^{1+\beta}\partial_{\tau_{\mathrm{r}}}c_0^e-\nabla_{\mathbf{y}}\cdot[(\mathbf{D}^e+\varepsilon^{-\alpha}\lambda t_+^2\mathbf{K}^e/c_0^e)(\nabla_{\mathbf{x}}c_0^e+\nabla_{\mathbf{y}}c_1^e)\\
&+2\varepsilon^{-\alpha}t_+\mathbf{K}^e(\nabla_{\mathbf{x}}\phi_0^e+\nabla_{\mathbf{y}}\phi_1^e)]=0,\quad \mathbf{y}\in\mathcal{B},
\end{aligned}\tag{A17}$$

subject to the interface condition

$$\begin{aligned}
&\mathbf{n}_e\cdot[(\mathbf{D}^e+\varepsilon^{-\alpha}\lambda t_+^2\mathbf{K}^e/c_0^e)(\nabla_{\mathbf{x}}c_0^e+\nabla_{\mathbf{y}}c_1^e)\\
&+2\varepsilon^{-\alpha}t_+\mathbf{K}^e(\nabla_{\mathbf{x}}\phi_0^e+\nabla_{\mathbf{y}}\phi_1^e)]=2\varepsilon^{\beta}A_0B_0,\quad \mathbf{y}\in\Gamma.
\end{aligned}\tag{A18}$$

Integrating (A17) over $\mathcal{B}$ with respect to $\mathbf{y}$, while accounting for the boundary condition (A18), and the periodicity of the coefficients on the external boundary of the unit cell ∂Y, we obtain

$$\varepsilon^{1+\beta}\partial_{\tau_{\mathrm{r}}e}c_0^e=2\varepsilon^{\beta}\mathcal{K}^\star A_0B_0,\tag{A19}$$

where $\mathcal{K}^\star$ is defined by (23).

Combining (A19) with (A17) to eliminate the temporal derivative, we obtain

$$\begin{aligned}
&2\varepsilon^{\beta}\mathcal{K}^\star A_0B_0-\nabla_{\mathbf{y}}\cdot[(\mathbf{D}^e+\varepsilon^{-\alpha}\lambda t_+^2\mathbf{K}^e/c_0^e)(\nabla_{\mathbf{x}}c_0^e+\nabla_{\mathbf{y}}c_1^e)\\
&+2\varepsilon^{-\alpha}t_+\mathbf{K}^e(\nabla_{\mathbf{x}}\phi_0^e+\nabla_{\mathbf{y}}\phi_1^e)]=0.
\end{aligned}\tag{A20}$$

Similarly, the charge balance equation (A9) at $\mathcal{O}(\varepsilon^{-1})$ is

$$\nabla_{\mathbf{y}}\cdot[\lambda t_+\mathbf{K}^e/c_0^e(\nabla_{\mathbf{x}}c_0^e+\nabla_{\mathbf{y}}c_1^e)+2\mathbf{K}^e(\nabla_{\mathbf{x}}\phi_0^e+\nabla_{\mathbf{y}}\phi_1^e)]=0,\quad \mathbf{y}\in\mathcal{B},\tag{A21}$$

subject to

$$\mathbf{n}_e\cdot[\varepsilon^{-\alpha}\lambda t_+\mathbf{K}^e/c_0^e(\nabla_{\mathbf{x}}c_0^e+\nabla_{\mathbf{y}}c_1^e)+2\varepsilon^{-\alpha}\mathbf{K}^e(\nabla_{\mathbf{x}}\phi_0^e+\nabla_{\mathbf{y}}\phi_1^e)-2\varepsilon^{\beta}A_0B_0]=0,\tag{A22}$$

for $\mathbf{y}\in\Gamma$. Equations (A18), (A20), (A21) and (A22) form boundary value problems for both c_1^e and ϕ_1^e. Following Ref. 64 and Ref. 27 (pp. 10, Eqs. 3.6–3.7), we look for solutions in the form

$$\begin{aligned}
c_1^e(\mathbf{x},\mathbf{y},t,\tau_{\mathrm{r}},\tau_{me},\tau_{ms})&=\boldsymbol{\chi}_1(\mathbf{y})\cdot\nabla_{\mathbf{x}}c_0^e(\mathbf{x},t,\tau_{\mathrm{r}},\tau_{me},\tau_{ms})+\overline{c}_1^e(\mathbf{x},t,\tau_{\mathrm{r}},\tau_{me},\tau_{ms}),\\
\phi_1^e(\mathbf{x},\mathbf{y},t,\tau_{\mathrm{r}},\tau_{me},\tau_{ms})&=\boldsymbol{\chi}_2(\mathbf{y})\cdot\nabla_{\mathbf{x}}\phi_0^e(\mathbf{x},t,\tau_{\mathrm{r}},\tau_{me},\tau_{ms})+\overline{\phi}_1^e(\mathbf{x},t,\tau_{\mathrm{r}},\tau_{me},\tau_{ms}).
\end{aligned}\tag{A23}$$

Substitution of (A23) into (A20) and (A18) leads to

$$\begin{aligned}
&2\varepsilon^{\beta}\mathcal{K}^\star A_0B_0-\nabla_{\mathbf{y}}\cdot[(\mathbf{D}^e+\varepsilon^{-\alpha}\lambda t_+^2\mathbf{K}^e/c_0^e)(\mathbf{I}+\nabla_{\mathbf{y}}\boldsymbol{\chi}_1)\nabla_{\mathbf{x}}c_0^e\\
&+2\varepsilon^{-\alpha}t_+\mathbf{K}^e(\mathbf{I}+\nabla_{\mathbf{y}}\boldsymbol{\chi}_2)\nabla_{\mathbf{x}}\phi_0^e]=0,\quad \mathbf{y}\in\mathcal{B},
\end{aligned}\tag{A24a}$$

subject to $\langle\boldsymbol{\chi}_1\rangle_e=\langle\boldsymbol{\chi}_2\rangle_e=0$ and

$$\begin{aligned}
&\mathbf{n}_e\cdot[(\mathbf{D}^e+\varepsilon^{-\alpha}\lambda t_+^2\mathbf{K}^e/c_0^e)(\mathbf{I}+\nabla_{\mathbf{y}}\boldsymbol{\chi}_1)\nabla_{\mathbf{x}}c_0^e\\
&+2\varepsilon^{-\alpha}t_+\mathbf{K}^e(\mathbf{I}+\nabla_{\mathbf{y}}\boldsymbol{\chi}_2)\nabla_{\mathbf{x}}\phi_0^e]=2\varepsilon^{\beta}A_0B_0\qquad \mathbf{y}\in\Gamma,
\end{aligned}\tag{A24b}$$

where $\mathbf{I}$ is the identity matrix, and $\boldsymbol{\chi}_1$ and $\boldsymbol{\chi}_2$ are periodic vector fields. Substitution of (A23) into (A21) and (A22) leads to

$$\nabla_{\mathbf{y}}\cdot[\lambda t_+\mathbf{K}^e/c_0^e(\mathbf{I}+\nabla_{\mathbf{y}}\boldsymbol{\chi}_1)\nabla_{\mathbf{x}}c_0^e+2\mathbf{K}^e(\mathbf{I}+\nabla_{\mathbf{y}}\boldsymbol{\chi}_2)\nabla_{\mathbf{x}}\phi_0^e]=0,\tag{A25a}$$

subject to

$$\mathbf{n}_e\cdot[\varepsilon^{-\alpha}\lambda t_+\mathbf{K}^e/c_0^e(\mathbf{I}+\nabla_{\mathbf{y}}\boldsymbol{\chi}_1)\nabla_{\mathbf{x}}c_0^e+2\varepsilon^{-\alpha}\mathbf{K}^e(\mathbf{I}+\nabla_{\mathbf{y}}\boldsymbol{\chi}_2)\nabla_{\mathbf{x}}\phi_0^e-2\varepsilon^{\beta}A_0B_0]=0,\tag{A25b}$$

Equations (A24) and (A25) define the closure variables $\boldsymbol{\chi}_1(\mathbf{y})$ and $\boldsymbol{\chi}_2(\mathbf{y})$. The coupling of $\boldsymbol{\chi}_1(\mathbf{y})$ and $\boldsymbol{\chi}_2(\mathbf{y})$ with $c_0^e(\mathbf{x})$, $\phi_0^e(\mathbf{x})$, $A_0(\mathbf{x})$ and $B_0(\mathbf{x})$ through the boundary value problems (A24) and (A25) is incompatible with the closure variables' general representation postulated in (A23). This inconsistency is resolved by imposing the following constraints on the exponents α and β. If we choose $\beta>\max\{0,-\alpha\}$ and $\alpha<0$, then the term $\mathcal{K}^\star A_0B_0$ is negligible relative to the smallest term in (A24) and the nonlinear migration term $\varepsilon^{-\alpha}\lambda t_+^2\mathbf{K}^e/c_0^e$ relative to $\mathbf{D}^e$. Under these constraints, (A24) and (A25) simplify to

$$\nabla_{\mathbf{y}}\cdot[\mathbf{D}^e(\mathbf{I}+\nabla_{\mathbf{y}}\boldsymbol{\chi}_1)\nabla_{\mathbf{x}}c_0^e]=0\qquad \mathbf{y}\in\mathcal{B},\tag{A26a}$$

$$\mathbf{n}_e\cdot[\mathbf{D}^e(\mathbf{I}+\nabla_{\mathbf{y}}\boldsymbol{\chi}_1)\nabla_{\mathbf{x}}c_0^e]=0\qquad \mathbf{y}\in\Gamma,\tag{A26b}$$

Equation (A26) can be satisfied for all $\mathbf{x}\in\Omega$ if

$$\nabla_{\mathbf{y}}\cdot[\mathbf{D}^e(\mathbf{I}+\nabla_{\mathbf{y}}\boldsymbol{\chi}_1)]=0,\qquad \mathbf{y}\in\mathcal{B}\tag{A27a}$$

$$\mathbf{n}_e\cdot[\mathbf{D}^e(\mathbf{I}+\nabla_{\mathbf{y}}\boldsymbol{\chi}_1)]=0,\qquad \mathbf{y}\in\Gamma.\tag{A27b}$$

Similarly, (A25) yields

$$\nabla_{\mathbf{y}}\cdot[\lambda t_+\mathbf{K}^e(\mathbf{I}+\nabla_{\mathbf{y}}\boldsymbol{\chi}_1)]=0,\qquad \mathbf{y}\in\mathcal{B}\tag{A28a}$$

$$\mathbf{n}_e\cdot[\lambda t_+\mathbf{K}^e(\mathbf{I}+\nabla_{\mathbf{y}}\boldsymbol{\chi}_1)]=0,\qquad \mathbf{y}\in\Gamma\tag{A28b}$$

and

$$\nabla_{\mathbf{y}}\cdot[\mathbf{K}^e(\mathbf{I}+\nabla_{\mathbf{y}}\boldsymbol{\chi}_2)]=0,\qquad \mathbf{y}\in\mathcal{B},\tag{A29a}$$

$$\mathbf{n}_e\cdot[\mathbf{K}^e(\mathbf{I}+\nabla_{\mathbf{y}}\boldsymbol{\chi}_2)]=0,\qquad \mathbf{y}\in\Gamma.\tag{A29b}$$

Consistency of (A27) with (A28) implies

$$\nabla_{\mathbf{y}}\cdot(\mathbf{I}+\nabla_{\mathbf{y}}\boldsymbol{\chi}_1)=0,\qquad \mathbf{y}\in\mathcal{B}\tag{A30a}$$

$$\mathbf{n}_e\cdot(\mathbf{I}+\nabla_{\mathbf{y}}\boldsymbol{\chi}_1)=0,\qquad \mathbf{y}\in\Gamma\tag{A30b}$$

In (A29), the conductivity tensor $\mathbf{K}^e$ is a function of concentration c^e and potential ϕ^e. With an order ε approximation $\mathbf{K}^e\approx\mathbf{K}^e(c_0^e,\phi_0^e)$. Then, (A29) can be simplified to

$$\nabla_{\mathbf{y}}\cdot(\mathbf{I}+\nabla_{\mathbf{y}}\boldsymbol{\chi}_2)=0,\qquad \mathbf{y}\in\mathcal{B},\tag{A31a}$$

$$\mathbf{n}_e\cdot(\mathbf{I}+\nabla_{\mathbf{y}}\boldsymbol{\chi}_2)=0,\qquad \mathbf{y}\in\Gamma.\tag{A31b}$$

As a result, $\boldsymbol{\chi}_1(\mathbf{y})=\boldsymbol{\chi}_2(\mathbf{y})=:\boldsymbol{\chi}^e(\mathbf{y})$. The treatment of the closure variable is consistent with the approach employed in Ref. 65. The closure variable $\boldsymbol{\chi}^e(\mathbf{y})$ defines the cell problem and describes the behavior of the effective diffusion and conductivity tensors.

Recalling the definitions of Da_e and Pe_e in (19) allows us to reformulate the conditions in terms of α and β in the form of constraints 2)–4) for the electrolyte. Having identified the conditions that guarantee homogenizability, we proceed to derive the effective mass transport equation (20).

Terms of order $\mathcal{O}(1)$.— Collecting the zeroth-order term in the mass balance equation (A5) and first-order term in the corresponding boundary condition (A7), we obtain

$$\begin{aligned}&\partial_t c_0^e + \varepsilon^{-\alpha}(\partial_{\tau_{me}} c_0^e + \varepsilon^{\beta-\gamma}\partial_{\tau_{ms}} c_0^e) + \varepsilon^{1+\beta}\partial_{\tau_r} c_1^e\\ &- \nabla_{\mathbf{x}}\cdot[(\mathbf{D}^e + \varepsilon^{-\alpha}\lambda t_+^2 \mathbf{K}^e/c_0^e)(\nabla_{\mathbf{x}} c_0^e + \nabla_{\mathbf{y}} c_1^e) + 2\varepsilon^{-\alpha} t_+ \mathbf{K}^e(\nabla_{\mathbf{x}}\phi_0^e + \nabla_{\mathbf{y}}\phi_1^e)]\\ &- \nabla_{\mathbf{y}}\cdot[(\mathbf{D}^e + \varepsilon^{-\alpha}\lambda t_+^2 \mathbf{K}^e/c_0^e)(\nabla_{\mathbf{x}} c_1^e + \nabla_{\mathbf{y}} c_2^e) + 2\varepsilon^{-\alpha} t_+ \mathbf{K}^e(\nabla_{\mathbf{x}}\phi_1^e + \nabla_{\mathbf{y}}\phi_2^e)\\ &- \varepsilon^{-\alpha}\lambda t_+^2 \mathbf{K}^e(c_1^e/c_0^e)/c_0^e(\nabla_{\mathbf{x}} c_0^e + \nabla_{\mathbf{y}} c_1^e)] = 0 \qquad \text{[A32]}\end{aligned}$$

subject to

$$\begin{aligned}&\mathbf{n}_e\cdot[(\mathbf{D}^e + \varepsilon^{-\alpha}\lambda t_+^2 \mathbf{K}^e/c_0^e)(\nabla_{\mathbf{x}} c_1^e + \nabla_{\mathbf{y}} c_2^e) + 2\varepsilon^{-\alpha} t_+ \mathbf{K}^e(\nabla_{\mathbf{x}}\phi_1^e + \nabla_{\mathbf{y}}\phi_2^e)\\ &- \varepsilon^{-\alpha}\lambda t_+^2 \mathbf{K}^e/c_0^e(c_1^e/c_0^e)(\nabla_{\mathbf{x}} c_0^e + \nabla_{\mathbf{y}} c_1^e) = 2\varepsilon^{\beta}(A_0 B_1 + A_1 B_0)] \qquad \text{[A33]}\end{aligned}$$

since $\nabla_{\mathbf{y}} c_0^e = 0$. Integrating (A32) over $\mathcal{B}$ with respect to $\mathbf{y}$ and using the boundary condition (A33) leads to

$$\begin{aligned}&\partial_t\langle c_0^e\rangle_{\mathcal{B}} + \varepsilon^{-\alpha}(\partial_{\tau_{me}}\langle c_0^e\rangle_{\mathcal{B}} + \varepsilon^{\beta-\gamma}\partial_{\tau_{ms}}\langle c_0^e\rangle_{\mathcal{B}}) + \varepsilon^{1+\beta}\partial_{\tau_r}\langle c_1^e\rangle_{\mathcal{B}}\\ &- \eta^{-1}\nabla_{\mathbf{x}}\cdot[(\mathbf{D}^{e\star\star} + \varepsilon^{-\alpha}\lambda t_+^2 \mathbf{K}^{e\star\star}/\langle c_0^e\rangle_{\mathcal{B}})\nabla_{\mathbf{x}}\langle c_0^e\rangle_{\mathcal{B}} + 2\varepsilon^{-\alpha} t_+ \mathbf{K}^{e\star\star}\nabla_{\mathbf{x}}\langle\phi_0^e\rangle_{\mathcal{B}}]\\ &- 2\varepsilon^{\beta}\mathcal{K}^\star(\langle A_0\rangle_{\mathcal{B}}\langle B_1\rangle_\Gamma + \langle A_1\rangle_\Gamma\langle B_0\rangle_{\mathcal{B}}) = 0 \qquad \text{[A34]}\end{aligned}$$

where $\mathcal{K}^\star = |\Gamma|/|\mathcal{B}|$, $\mathbf{D}^{e\star\star} = \langle\mathbf{D}^e(\mathbf{I} + \nabla_{\mathbf{y}}\boldsymbol{\chi}^e)\rangle_e$, $\mathbf{K}^{e\star\star} = \langle\mathbf{K}^e(\mathbf{I} + \nabla_{\mathbf{y}}\boldsymbol{\chi}^e)\rangle_e$ and

$$\langle A_1\rangle_\Gamma = (\langle\phi_1^s\rangle_\Gamma - \langle\phi_1^e\rangle_\Gamma)\cosh(\langle\phi_0^s\rangle_{\mathcal{B}} - \langle\phi_0^e\rangle_{\mathcal{B}} - U), \qquad \text{[A35a]}$$

$$\langle B_1\rangle_\Gamma = \sqrt{\langle c_0^e\rangle_{\mathcal{B}}\langle c_0^s\rangle_{\mathcal{B}}(1-\langle c_0^s\rangle_{\mathcal{B}})}\left[\frac{\langle c_1^s\rangle_\Gamma}{2\langle c_0^s\rangle_{\mathcal{B}}} + \frac{\langle c_1^e\rangle_\Gamma}{2\langle c_0^e\rangle_{\mathcal{B}}} - \frac{\langle c_1^s\rangle_\Gamma}{2(1-\langle c_0^s\rangle_{\mathcal{B}})}\right]. \qquad \text{[A35b]}$$

Next, we recall that

$$\begin{aligned}\langle c^e\rangle_{\mathcal{B}} &= \langle c_0^e\rangle_{\mathcal{B}} + \varepsilon\langle c_1^e\rangle_{\mathcal{B}} + \mathcal{O}(\varepsilon^2),\\ \langle\phi^e\rangle_{\mathcal{B}} &= \langle\phi_0^e\rangle_{\mathcal{B}} + \varepsilon\langle\phi_1^e\rangle_{\mathcal{B}} + \mathcal{O}(\varepsilon^2).\end{aligned} \qquad \text{[A36]}$$

Multiplying the temporal derivative of (A36) by ε, we obtain

$$\varepsilon\partial_t\langle c^e\rangle_{\mathcal{B}} = \varepsilon\partial_t\langle c_0^e\rangle_{\mathcal{B}} + \varepsilon^{1+\beta}\partial_{\tau_r}\langle c_0^e\rangle_{\mathcal{B}} + \varepsilon^{1-\alpha}(\partial_{\tau_{me}}\langle c_0^e\rangle_{\mathcal{B}} + \varepsilon^{\beta-\gamma}\partial_{\tau_{ms}}\langle c_0^e\rangle_{\mathcal{B}}) + \mathcal{O}(\varepsilon^2). \qquad \text{[A37]}$$

Multiplying (A34) by ε, adding the result to (A19), and using (A37), we obtain

$$\begin{aligned}\varepsilon\partial_t\langle c^e\rangle_{\mathcal{B}} = \varepsilon\eta^{-1}\nabla_{\mathbf{x}}\cdot[(\mathbf{D}^{e\star\star} + \varepsilon^{-\alpha}\lambda t_+^2\mathbf{K}^{e\star\star}/\langle c_0^e\rangle_{\mathcal{B}})\nabla_{\mathbf{x}}\langle c_0^e\rangle_{\mathcal{B}} + 2\varepsilon^{-\alpha} t_+\mathbf{K}^{e\star\star}\nabla_{\mathbf{x}}\langle\phi_0^e\rangle_{\mathcal{B}}]\\ + 2\varepsilon^{\beta}\mathcal{K}^\star[\langle A_0\rangle_{\mathcal{B}}\langle B_0\rangle_{\mathcal{B}} + \varepsilon(\langle A_0\rangle_{\mathcal{B}}\langle B_1\rangle_\Gamma + \langle A_1\rangle_\Gamma\langle B_0\rangle_{\mathcal{B}})] \qquad \text{[A38]}\end{aligned}$$

Combining this result with the expansions $\varepsilon\langle c^e\rangle_{\mathcal{B}} = \varepsilon\langle c_0^e\rangle_{\mathcal{B}} + \mathcal{O}(\varepsilon^2) = \varepsilon c_0^e + \mathcal{O}(\varepsilon^2)$ and $\varepsilon\langle\phi^e\rangle_{\mathcal{B}} = \varepsilon\langle\phi_0^e\rangle_{\mathcal{B}} + \mathcal{O}(\varepsilon^2) = \varepsilon\phi_0^e + \mathcal{O}(\varepsilon^2)$ while recalling the definitions of Da_e and Pe_e in (19) and assuming $\langle\psi^s\rangle_\Gamma \approx \langle\psi^s\rangle_s$ and $\langle\psi^e\rangle_\Gamma \approx \langle\psi^e\rangle_{\mathcal{B}}$, where $\psi = \{c, \phi\}$, leads to

$$\begin{aligned}\eta\partial_t\langle c^e\rangle_{\mathcal{B}} = \nabla_{\mathbf{x}}\cdot[(\mathbf{D}^{e\star\star} + \varepsilon^{-\alpha}\lambda t_+^2\mathbf{K}^{e\star\star}/\langle c^e\rangle_{\mathcal{B}})\nabla_{\mathbf{x}}\langle c^e\rangle_{\mathcal{B}} + 2\varepsilon^{-\alpha} t_+\mathbf{K}^{e\star\star}\nabla_{\mathbf{x}}\langle\phi^e\rangle_{\mathcal{B}}]\\ + 2\eta\varepsilon^{-1}\mathcal{K}^\star\mathrm{Da}_e f(\langle c^e\rangle_{\mathcal{B}}, \langle c^s\rangle_s, \langle\phi^e\rangle_{\mathcal{B}}, \langle\phi^s\rangle_s), \qquad \text{[A39]}\end{aligned}$$

since

$$f(\langle c^e\rangle_{\mathcal{B}}, \langle c^s\rangle_s, \langle\phi^e\rangle_{\mathcal{B}}, \langle\phi^s\rangle_s) \approx \langle A_0\rangle_{\mathcal{B}}\langle B_0\rangle_{\mathcal{B}} + \varepsilon(\langle A_0\rangle_{\mathcal{B}}\langle B_1\rangle_\Gamma + \langle A_1\rangle_\Gamma\langle B_0\rangle_{\mathcal{B}}) + \mathcal{O}(\varepsilon^2) \qquad \text{[A40]}$$

where $f(\langle c^e\rangle_{\mathcal{B}}, \langle c^s\rangle_s, \langle\phi^e\rangle_{\mathcal{B}}, \langle\phi^s\rangle_s)$ is defined by (22).

Similarly, collecting $\mathcal{O}(1)-$terms in the charge balance equation in the electrolyte (A9) and $\mathcal{O}(\varepsilon)-$terms in the boundary condition (A10) while accounting for $\nabla_{\mathbf{y}} c_0^e = 0$, we obtain

$$\begin{aligned}&\nabla_{\mathbf{x}}\cdot[\lambda t_+\mathbf{K}^e/c_0^e(\nabla_{\mathbf{x}} c_0^e + \nabla_{\mathbf{y}} c_1^e) + 2\mathbf{K}^e(\nabla_{\mathbf{x}}\phi_0^e + \nabla_{\mathbf{y}}\phi_1^e)\\ &+ \nabla_{\mathbf{y}}\cdot[\lambda t_+\mathbf{K}^e/c_0^e(\nabla_{\mathbf{x}} c_1^e + \nabla_{\mathbf{y}} c_2^e) - \lambda t_+\mathbf{K}^e(c_1^e/c_0^e)/c_0^e(\nabla_{\mathbf{x}} c_0^e + \nabla_{\mathbf{y}} c_1^e)\\ &+ 2\mathbf{K}^e(\nabla_{\mathbf{x}}\phi_1^e + \nabla_{\mathbf{y}}\phi_2^e)] = 0, \qquad \text{[A41]}\end{aligned}$$

subject to

$$\begin{aligned}&\mathbf{n}_e\cdot[\lambda t_+\mathbf{K}^e/c_0^e(\nabla_{\mathbf{x}} c_1^e + \nabla_{\mathbf{y}} c_2^e) - \lambda t_+\mathbf{K}^e/c_0(c_1/c_0)(\nabla_{\mathbf{x}} c_0^e + \nabla_{\mathbf{y}} c_1^e)\\ &+ 2\mathbf{K}^e(\nabla_{\mathbf{x}}\phi_1^e + \nabla_{\mathbf{y}}\phi_2^e)] = 2\varepsilon^{\alpha+\beta}(A_0 B_1 + A_1 B_0). \qquad \text{[A42]}\end{aligned}$$

We multiply by ε both Equation (A41) and its boundary condition (A42), add them to (A21) and (A22), respectively, and integrate the resulting equation over $\mathcal{B}$ while employing the newly obtained boundary conditions. This leads to

$$\begin{aligned}\varepsilon^{1-\alpha}\eta^{-1}\nabla_{\mathbf{x}}\cdot[(\lambda t_+\mathbf{K}^{e\star\star}/\langle c_0^e\rangle_{\mathcal{B}})\nabla_{\mathbf{x}}\langle c_0^e\rangle_{\mathcal{B}} + 2\mathbf{K}^{e\star\star}\nabla_{\mathbf{x}}\langle\phi_0^e\rangle_{\mathcal{B}}]\\ = 2\varepsilon^{\beta}\mathcal{K}^\star[\langle A_0\rangle_{\mathcal{B}}\langle B_0\rangle_{\mathcal{B}} + \varepsilon(\langle A_0\rangle_{\mathcal{B}}\langle B_1\rangle_\Gamma + \langle A_1\rangle_\Gamma\langle B_0\rangle_{\mathcal{B}})] \qquad \text{[A43]}\end{aligned}$$

where $\mathbf{K}^{e\star\star} = \langle\mathbf{K}^e(\mathbf{I} + \nabla_{\mathbf{y}}\boldsymbol{\chi}^e)\rangle_e$. Following a similar procedure to that outlined for the mass transport equation, (A43) can be written as

$$\begin{aligned}\mathrm{Pe}_e\nabla_{\mathbf{x}}\cdot[(\lambda t_+\mathbf{K}^{e\star\star}/\langle c^e\rangle_{\mathcal{B}})\nabla_{\mathbf{x}}\langle c^e\rangle_{\mathcal{B}} + 2\mathbf{K}^{e\star\star}\nabla_{\mathbf{x}}\langle\phi^e\rangle_{\mathcal{B}}]\\ = 2\eta\varepsilon^{-1}\mathcal{K}^\star\mathrm{Da}_e f(\langle c^e\rangle_{\mathcal{B}}, \langle c^s\rangle_s, \langle\phi^e\rangle_{\mathcal{B}}, \langle\phi^s\rangle_s), \qquad \text{[A44]}\end{aligned}$$

where $f(\langle c^e\rangle_{\mathcal{B}}, \langle c^s\rangle_s, \langle\phi^e\rangle_{\mathcal{B}}, \langle\phi^s\rangle_s)$ is defined by (22).

Equations (A39) and (A44) govern the dynamics of $\langle c^e\rangle_{\mathcal{B}}$ and $\langle\phi^e\rangle_{\mathcal{B}}$ in the electrolyte up to errors of order ε^2.

Appendix B: Homogenization in the Electrode

We follow the same procedure as outlined in Appendix A. We report the derivations for completeness. We set $c_\varepsilon^j(\mathbf{x}, t) = c^j(\mathbf{x}, \mathbf{y}, t, \tau_r, \tau_{me}, \tau_{ms})$ and $\phi_\varepsilon^j(\mathbf{x}, t) = \phi^j(\mathbf{x}, \mathbf{y}, t, \tau_r, \tau_{me}, \tau_{ms})$, $j = \{e, s\}$. Then, combining (17) with (11) and (12) we obtain

$$\begin{aligned}&\frac{\partial c^s}{\partial t} + \mathrm{Da}_e\frac{\partial c^s}{\partial\tau_r} + \mathrm{Pe}_e\left(\frac{\partial c^s}{\partial\tau_{me}} + \frac{\mathrm{Da}_e}{\mathrm{Da}_s}\frac{\partial c^s}{\partial\tau_{ms}}\right) = \mathrm{Da}_e\mathrm{Da}_s^{-1}\nabla_{\mathbf{x}}\cdot[\mathbf{D}^s(\nabla_{\mathbf{x}} c^s + \varepsilon^{-1}\nabla_{\mathbf{y}} c^s)]\\ &+ \varepsilon^{-1}\mathrm{Da}_e\mathrm{Da}_s^{-1}\nabla_{\mathbf{y}}\cdot[\mathbf{D}^s(\nabla_{\mathbf{x}} c^s + \varepsilon^{-1}\nabla_{\mathbf{y}} c^s)], \quad \mathbf{x}\in\mathcal{S}^\varepsilon \qquad \text{[B1]}\end{aligned}$$

and

$$\nabla_{\mathbf{x}}\cdot[\mathbf{K}^s(\nabla_{\mathbf{x}}\phi^s + \varepsilon^{-1}\nabla_{\mathbf{y}}\phi^s)] + \varepsilon^{-1}\nabla_{\mathbf{y}}\cdot[\mathbf{K}^s(\nabla_{\mathbf{x}}\phi^s + \varepsilon^{-1}\nabla_{\mathbf{y}}\phi^s)] = 0, \quad \mathbf{x}\in\mathcal{S}^\varepsilon \qquad \text{[B2]}$$

subject to

$$-\mathbf{n}_s\cdot[\mathbf{D}^s(\nabla_{\mathbf{x}} c^s + \varepsilon^{-1}\nabla_{\mathbf{y}} c^s)] = \mathrm{Da}_s f(c_\varepsilon^e, c_\varepsilon^s, \phi_\varepsilon^s, \phi_\varepsilon^e), \quad \mathbf{x}\in\Gamma^\varepsilon \qquad \text{[B3]}$$

and

$$-\mathbf{n}_s\cdot[2\mathrm{Pe}_s\,\mathbf{K}^s(\nabla_{\mathbf{x}}\phi^s + \varepsilon^{-1}\nabla_{\mathbf{y}}\phi^s)] = \mathrm{Da}_s f(c_\varepsilon^e, c_\varepsilon^s, \phi_\varepsilon^s, \phi_\varepsilon^e), \quad \mathbf{x}\in\Gamma^\varepsilon \qquad \text{[B4]}$$

respectively, where $f(c_\varepsilon^e, c_\varepsilon^s, \phi_\varepsilon^s, \phi_\varepsilon^e)$ is defined in (10).

Mass and charge transport asymptotic expansions.— Substituting (18) and (19) into the mass transport equation in the electrode (B1), we obtain

$$\begin{aligned}&\varepsilon^{-2}\{-\varepsilon^{\beta-\gamma}\nabla_{\mathbf{y}}\cdot(\mathbf{D}^s\nabla_{\mathbf{y}} c_0^s)\}\\ &+ \varepsilon^{-1}\{\varepsilon^{1+\beta}\partial_{\tau_r} c_0^s - \varepsilon^{\beta-\gamma}\nabla_{\mathbf{x}}\cdot(\mathbf{D}^s\nabla_{\mathbf{y}} c_0^s) - \varepsilon^{\beta-\gamma}\nabla_{\mathbf{y}}\cdot[\mathbf{D}^s(\nabla_{\mathbf{x}} c_0^s + \nabla_{\mathbf{y}} c_1^s)]\}\\ &+ \varepsilon^0\{\partial_t c_0^s + \varepsilon^{-\alpha}(\partial_{\tau_{me}} c_0^s + \varepsilon^{\beta-\gamma}\partial_{\tau_{ms}} c_0^s) + \varepsilon^{1+\beta}\partial_{\tau_r} c_1^s - \varepsilon^{\beta-\gamma}\nabla_{\mathbf{x}}\cdot[\mathbf{D}^s(\nabla_{\mathbf{x}} c_0^s + \nabla_{\mathbf{y}} c_1^s)\\ &- \varepsilon^{\beta-\gamma}\nabla_{\mathbf{y}}\cdot[\mathbf{D}^s(\nabla_{\mathbf{x}} c_1^s + \nabla_{\mathbf{y}} c_2^s)]\} = \mathcal{O}(\varepsilon), \quad \mathbf{y}\in\mathcal{S}, \qquad \text{[B5]}\end{aligned}$$

subject to

$$\begin{aligned}&\varepsilon^{-1}\{\mathbf{n}_s\cdot(\mathbf{D}^s\nabla_{\mathbf{y}} c_0^s)\} + \varepsilon^0\{\mathbf{n}_s\cdot[\mathbf{D}^s(\nabla_{\mathbf{x}} c_0^s + \nabla_{\mathbf{y}} c_1^s)] + 2\varepsilon^\gamma A_0 B_0)\}\\ &+ \varepsilon\{\mathbf{n}_s\cdot[\mathbf{D}^s(\nabla_{\mathbf{x}} c_1^s + \nabla_{\mathbf{y}} c_2^s)] + 2\varepsilon^\gamma(A_0 B_1 + A_1 B_0)\}] = \mathcal{O}(\varepsilon^2), \quad \mathbf{y}\in\Gamma, \qquad \text{[B6]}\end{aligned}$$

where A_0, A_1, B_0 and B_1 are defined in (A8). Similarly, the charge transport equation (B2) and the boundary condition (B4) combined with (18) and (19) yield to

$$\begin{aligned}&\varepsilon^{-2}\{\nabla_{\mathbf{y}}\cdot(\mathbf{K}^s\nabla_{\mathbf{y}}\phi_0^s)\} + \varepsilon^{-1}\{\nabla_{\mathbf{x}}\cdot(\mathbf{K}^s\nabla_{\mathbf{y}}\phi_0^s) + \nabla_{\mathbf{y}}\cdot[\mathbf{K}^s(\nabla_{\mathbf{x}}\phi_0^s + \nabla_{\mathbf{y}}\phi_1^s)]\}\\ &+ \varepsilon^0\{\nabla_{\mathbf{x}}\cdot[\mathbf{K}^s(\nabla_{\mathbf{x}}\phi_0^s + \nabla_{\mathbf{y}}\phi_1^s) + \nabla_{\mathbf{y}}\cdot[\mathbf{K}^s(\nabla_{\mathbf{x}}\phi_1^s + \nabla_{\mathbf{y}}\phi_2^s)]\} = \mathcal{O}(\varepsilon), \quad \mathbf{y}\in\mathcal{S}, \qquad \text{[B7]}\end{aligned}$$

subject to

$$\begin{aligned}&\varepsilon^{-1}\{\mathbf{n}_s\cdot(\varepsilon^{-\delta}\mathbf{K}^s\nabla_{\mathbf{y}}\phi_0^s)\} + \varepsilon^0\{\mathbf{n}_s\cdot[\varepsilon^{-\delta}\mathbf{K}^s(\nabla_{\mathbf{x}}\phi_0^s + \nabla_{\mathbf{y}}\phi_1^s)] + 2\varepsilon^\gamma A_0 B_0\}\\ &+ \varepsilon\{\mathbf{n}_s\cdot[\varepsilon^{-\delta}\mathbf{K}^s(\nabla_{\mathbf{x}}\phi_1^s + \nabla_{\mathbf{y}}\phi_2^s)] + 2\varepsilon^\gamma(A_0 B_1 + A_1 B_0)\}] = \mathcal{O}(\varepsilon^2), \quad \mathbf{y}\in\Gamma, \qquad \text{[B8]}\end{aligned}$$

Terms of order $\mathcal{O}(\varepsilon^{-2})$.— Collecting the leading-order terms in the mass transport equation and corresponding boundary conditions (B5) and (B6), we obtain

$$\nabla_{\mathbf{y}}\cdot(\mathbf{D}^s\nabla_{\mathbf{y}} c_0^s) = 0, \qquad \mathbf{y}\in\mathcal{S}, \qquad \text{[B9]}$$

subject to the interface condition

$$\mathbf{n}_s\cdot(\mathbf{D}^s\nabla_{\mathbf{y}} c_0^s) = 0, \qquad \mathbf{y}\in\Gamma. \qquad \text{[B10]}$$

Similarly, at the leading order the charge balance equation (B7) and the boundary condition yield

$$\nabla_{\mathbf{y}}\cdot(\mathbf{K}^s\nabla_{\mathbf{y}}\phi_0^s) = 0, \qquad \mathbf{y}\in\mathcal{S}, \qquad \text{[B11]}$$

subject to

$$\mathbf{n}_s\cdot(\mathbf{K}^s\nabla_{\mathbf{y}}\phi_0^s) = 0, \qquad \mathbf{y}\in\Gamma. \qquad \text{[B12]}$$

The homogeneity of Equations (B9)–(B12) ensures that the above boundary value problems have both a trivial solution, i.e.

$$c_0^s = c_0^s(\mathbf{x}, t, \tau_r, \tau_{re}, \tau_{rs}), \quad [B13a]$$

$$\phi_0^s = \phi_0^s(\mathbf{x}, t, \tau_r, \tau_{re}, \tau_{rs}). \quad [B13b]$$

Terms of order $\mathcal{O}(\varepsilon^{-1})$.— At the following order, the mass transport equation (B5) can be written as

$$\varepsilon^{1+\gamma}\partial_{\tau_r} c_0^s - \nabla_{\mathbf{y}} \cdot [\mathbf{D}^s(\nabla_{\mathbf{x}} c_0^s + \nabla_{\mathbf{y}} c_1^s)] = 0, \quad \mathbf{y} \in \mathcal{S}, \quad [B14]$$

since $\nabla_{\mathbf{y}} c_0^s \equiv \mathbf{0}$, and it is subject to the boundary condition

$$\mathbf{n}_s \cdot [\mathbf{D}^s(\nabla_{\mathbf{x}} c_0^s + \nabla_{\mathbf{y}} c_1^s)] + 2\varepsilon^{\gamma} A_0 B_0 = 0, \quad \mathbf{y} \in \Gamma. \quad [B15]$$

Integrating (B14) over $\mathcal{S}$ with respect to $\mathbf{y}$, while accounting for the boundary condition (B15), and the periodicity of the coefficients on the external boundary of the unit cell ∂Y, we obtain

$$\varepsilon^{1+\gamma}\partial_{\tau_r} c_0^s = -2\eta\varepsilon^{\gamma}\mathcal{K}^{\star} A_0 B_0. \quad [B16]$$

We combine (B16) with (B14) to eliminate the temporal derivative and obtain

$$\nabla_{\mathbf{y}} \cdot [\mathbf{D}^s(\nabla_{\mathbf{x}} c_0^s + \nabla_{\mathbf{y}} c_1^s)] + 2\eta\varepsilon^{\gamma}\mathcal{K}^{\star} A_0 B_0 = 0. \quad [B17]$$

Similarly, the order $\mathcal{O}(\varepsilon^{-1})$ of the charge balance equation (B7) can be simplified to

$$\nabla_{\mathbf{y}} \cdot [\mathbf{K}^s(\nabla_{\mathbf{x}} \phi_0^s + \nabla_{\mathbf{y}} \phi_1^s)] = 0, \quad \mathbf{y} \in \mathcal{S}, \quad [B18]$$

subject to

$$\mathbf{n}_s \cdot [\varepsilon^{-\delta}\mathbf{K}^s(\nabla_{\mathbf{x}} \phi_0^s + \nabla_{\mathbf{y}} \phi_1^s)] + 2\varepsilon^{\gamma} A_0 B_0 = 0, \quad \mathbf{y} \in \Gamma. \quad [B19]$$

Equations (B17) and (B18) subject to (B15) and (B19) form a boundary value problem for c_1^s and ϕ_1^s, respectively. As outlined in Appendix A, we look for a solution in the form

$$\begin{aligned} c_1^s(\mathbf{x}, \mathbf{y}, t, \tau_r, \tau_{me}, \tau_{ms}) &= \boldsymbol{\chi}_3(\mathbf{y}) \cdot \nabla_{\mathbf{x}} c_0^s(\mathbf{x}, t, \tau_r, \tau_{me}, \tau_{ms}) + \overline{c}_1^s(\mathbf{x}, t, \tau_r, \tau_{me}, \tau_{ms}), \\ \phi_1^s(\mathbf{x}, \mathbf{y}, t, \tau_r, \tau_{me}, \tau_{ms}) &= \boldsymbol{\chi}_4(\mathbf{y}) \cdot \nabla_{\mathbf{x}} \phi_0^s(\mathbf{x}, t, \tau_r, \tau_{me}, \tau_{ms}) + \overline{\phi}_1^s(\mathbf{x}, t, \tau_r, \tau_{me}, \tau_{ms}). \end{aligned} \quad [B20]$$

Substitution of (B20) into (B17) and (B15) leads to the following cell problem for the closure variable $\boldsymbol{\chi}_3(\mathbf{y})$,

$$2\eta\varepsilon^{\gamma}\mathcal{K}^{\star} A_0 B_0 + \nabla_{\mathbf{y}} \cdot [\mathbf{D}^s(\mathbf{I} + \nabla_{\mathbf{y}}\boldsymbol{\chi}_3)\nabla_{\mathbf{x}} c_0^s] = 0, \quad \mathbf{y} \in \mathcal{S}, \quad [B21a]$$

subject to $\langle \boldsymbol{\chi}_3 \rangle_s = 0$ and

$$\mathbf{n}_s \cdot [\mathbf{D}^s(\mathbf{I} + \nabla_{\mathbf{y}}\boldsymbol{\chi}_3)\nabla_{\mathbf{x}} c_0^s] + 2\varepsilon^{\gamma} A_0 B_0 = 0, \quad \mathbf{y} \in \Gamma. \quad [B21b]$$

The boundary-value problem (B21) couples the pore scale with the continuum scale, in the sense that the closure variable $\boldsymbol{\chi}_3(\mathbf{y})$—a solution of the pore-scale cell problem (B21)—is influenced by the continuum scale through its dependence on the macroscopic concentration $c_0^s(\mathbf{x})$. This coupling is incompatible with the general representation (B20). This inconsistency is resolved by imposing the following constraint on the exponent γ, namely $\gamma > 0$. This condition ensures that $\boldsymbol{\chi}_3$ is independent of c_0^s, and the cell problem (B21) can be simplified to

$$\nabla_{\mathbf{y}} \cdot [\mathbf{D}^s(\mathbf{I} + \nabla_{\mathbf{y}}\boldsymbol{\chi}_3)] = 0, \quad \mathbf{y} \in \mathcal{S}, \quad [B22a]$$

$$\mathbf{n}_s \cdot [\mathbf{D}^s(\mathbf{I} + \nabla_{\mathbf{y}}\boldsymbol{\chi}_3)] = 0, \quad \mathbf{y} \in \Gamma. \quad [B22b]$$

Similarly, substitution of (B20) into the $\mathcal{O}(\varepsilon^{-1})$-charge balance equation (B18) and its boundary condition (B19) leads to the following cell problem for the closure variable $\boldsymbol{\chi}_4(\mathbf{y})$,

$$\nabla_{\mathbf{y}} \cdot [\mathbf{K}^s(\mathbf{I} + \nabla_{\mathbf{y}}\boldsymbol{\chi}_4)\nabla_{\mathbf{x}} \phi_0^s] = 0, \quad \mathbf{y} \in \mathcal{S}, \quad [B23a]$$

subject to $\langle \boldsymbol{\chi}_4 \rangle_s = 0$ and

$$\mathbf{n}_s \cdot [\varepsilon^{-\delta}\mathbf{K}^s(\nabla_{\mathbf{y}}\boldsymbol{\chi}_4 + \mathbf{I})]\nabla_{\mathbf{x}} \phi_0^s] + \varepsilon^{\gamma}(A_0 B_0) = 0, \quad \mathbf{y} \in \Gamma, \quad [B23b]$$

where $\boldsymbol{\chi}_4(\mathbf{y})$ is a Y-periodic vector field. Separation between pore- and continuum-scales requires $\gamma + \delta > 0$. Under this condition (B23), simplifies to

$$\nabla_{\mathbf{y}} \cdot [\mathbf{K}^s(\mathbf{I} + \nabla_{\mathbf{y}}\boldsymbol{\chi}_4)] = 0, \quad \mathbf{y} \in \mathcal{S}, \quad [B24a]$$

$$\mathbf{n}_s \cdot [\mathbf{K}^s(\mathbf{I} + \nabla_{\mathbf{y}}\boldsymbol{\chi}_4)] = 0, \quad \mathbf{y} \in \Gamma. \quad [B24b]$$

In (B22) and (B24), the diffusion and conductivity tensors are functions of concentration c^e and potential ϕ^e. With an order ε approximation $\mathbf{D}^e \approx \mathbf{D}^e(c_0^e, \phi_0^e)$ and $\mathbf{K}^e \approx \mathbf{K}^e(c_0^e, \phi_0^e)$. Then, $\boldsymbol{\chi}_4 = \boldsymbol{\chi}_3 =: \boldsymbol{\chi}^s(\mathbf{y})$, where $\boldsymbol{\chi}^s$ is a solution of the closure problem

$$\nabla_{\mathbf{y}} \cdot (\mathbf{I} + \nabla_{\mathbf{y}}\boldsymbol{\chi}^s) = 0, \quad \mathbf{y} \in \mathcal{S}, \quad [B25a]$$

$$\mathbf{n}_s \cdot (\mathbf{I} + \nabla_{\mathbf{y}}\boldsymbol{\chi}^s) = 0, \quad \mathbf{y} \in \Gamma. \quad [B25b]$$

Terms of order $\mathcal{O}(\varepsilon^0)$.— At the leading order, the mass transport equation in the electrode (B5)

$$\begin{aligned} &\partial_t c_0^s + \varepsilon^{-\alpha}(\partial_{\tau_{me}} c_0^s + \varepsilon^{\beta-\gamma}\partial_{\tau_{ms}} c_0^s) + \varepsilon^{1+\beta}\partial_{\tau_r} c_1^s - \varepsilon^{\beta-\gamma}\nabla_{\mathbf{x}} \cdot [\mathbf{D}^s(\nabla_{\mathbf{x}} c_0^s + \nabla_{\mathbf{y}} c_1^s)] \\ &\quad - \varepsilon^{\beta-\gamma}\nabla_{\mathbf{y}} \cdot [\mathbf{D}^s(\nabla_{\mathbf{x}} c_1^s + \nabla_{\mathbf{y}} c_2^s)] = 0, \qquad \mathbf{y} \in \mathcal{S}, \end{aligned} \quad [B26]$$

subject to

$$\mathbf{n}_s \cdot [\mathbf{D}^s(\nabla_{\mathbf{x}} c_1^s + \nabla_{\mathbf{y}} c_2^s)] + 2\varepsilon^{\gamma}(A_0 B_1 + A_1 B_0) = 0, \qquad \mathbf{y} \in \Gamma. \quad [B27]$$

Integrating (B26) over $\mathcal{S}$ with respect to $\mathbf{y}$ and using the interface condition (B27) leads to

$$\begin{aligned} &\partial_t \langle c_0^s \rangle_s + \varepsilon^{-\alpha}(\partial_{\tau_{me}} \langle c_0^s \rangle_s + \varepsilon^{\beta-\gamma}\partial_{\tau_{ms}} \langle c_0^s \rangle_s) + \varepsilon^{1+\beta}\partial_{\tau_r} \langle c_1^s \rangle_s - \varepsilon^{\beta-\gamma}\nabla_{\mathbf{x}} \cdot (\mathbf{D}^{s\star\star}\nabla_{\mathbf{x}} c_0^s) \\ &\quad + 2\varepsilon^{\beta-\gamma}\eta\mathcal{K}^{\star}(\langle A_0 \rangle_{\mathcal{B}} \langle B_1 \rangle_{\Gamma} + \langle A_1 \rangle_{\Gamma} \langle B_0 \rangle_{\mathcal{B}}) = 0, \end{aligned} \quad [B28]$$

where $\mathbf{D}^{s\star\star} = \langle \mathbf{D}^s(\mathbf{I} + \nabla_{\mathbf{y}}\boldsymbol{\chi}^s) \rangle_s$. Similarly, the leading order of the charge transport equation is

$$\nabla_{\mathbf{x}} \cdot [\mathbf{K}^s(\nabla_{\mathbf{x}} \phi_0^s + \nabla_{\mathbf{y}} \phi_1^s) + \nabla_{\mathbf{y}} \cdot [\mathbf{K}^s(\nabla_{\mathbf{x}} \phi_1^s + \nabla_{\mathbf{y}} \phi_2^s)] = 0, \qquad \mathbf{y} \in \mathcal{S}, \quad [B29]$$

subject to

$$\mathbf{n}_s \cdot [\varepsilon^{-\delta}\mathbf{K}^s(\nabla_{\mathbf{x}} \phi_1^s + \nabla_{\mathbf{y}} \phi_2^s)] + 2\varepsilon^{\gamma}(A_0 B_1 + A_1 B_0) = 0, \qquad \mathbf{y} \in \Gamma. \quad [B30]$$

Multiplying both (B29) and (B30) by ε, adding them to (B14) and (B15), respectively, and then integrating over $\mathcal{S}$, we obtain

$$\varepsilon^{1-\delta}\nabla_{\mathbf{x}} \cdot (\mathbf{K}^{s\star\star}\nabla_{\mathbf{x}} \langle \phi_0^s \rangle_s) = \varepsilon^{\gamma}\eta\mathcal{K}^{\star}\langle A_0 \rangle_{\mathcal{B}} \langle B_1 \rangle_{\Gamma} + \langle A_1 \rangle_{\Gamma} \langle B_0 \rangle_{\mathcal{B}}), \quad [B31]$$

where $\mathbf{K}^{s\star\star} = \langle \mathbf{K}^s(\mathbf{I} + \nabla_{\mathbf{y}}\boldsymbol{\chi}^s) \rangle_s$.

Following the procedure outlined in Appendix A and assuming that $\langle \boldsymbol{\chi}^s \rangle_s \approx \langle \boldsymbol{\chi}^s \rangle_{\Gamma}$, Equations (B28) and (B31) lead to the macroscopic equations for mass and charge transport in the electrode (26) and (27), respectively.

References

1. V. R. Subramanian, V. D. Diwakar, and D. Tapriyal, "Efficient Macro-Micro Scale Coupled Modeling of Batteries," *J. Electrochem. Soc*, **152**(10), A2002 (2005).
2. K.-J. Lee, K. Smith, and G.-H. Kim, "A Three-Dimensional Thermal-Electrochemical Coupled Model for Spirally Wound Large-Format Lithium-Ion Batteries," April 2011. Slides of a talk given at the Space Power Workshop, Los Angeles, CA.
3. G. Richardson, G. Denuault, and C. P. Please, "Multiscale modeling and analysis of lithium-ion battery charge and discharge," *J. Eng. Math.*, **72**(1), 41, (2012).
4. V. Ramadesigan, P. W. C. Northrop, S. De, S. Santhanagopalan, R. D. Braatz, and V. R. Subramanian, "Modeling and Simulation of Lithium-Ion Batteries from a Systems Engineering Perspective," *J. Electrochem. Soc*, **159**(3), R31 (2012).
5. A. A. Franco, "Multiscale modeling and numerical simulation of rechargeable lithium ion batteries: concepts, methods and challenges," *RSC Adv.*, **3**, 13027 (2013).
6. J. Newman and W. Tiedemann, "Porous-Electrode Theory with Battery Applications," *AIChE J.*, **21**(1), 25 (1975).
7. M. Doyle, T. F. Fuller, and J. Newman, "Modeling of Galvanostatic Charge and Discharge of the Lithium/Polymer/Insertion Cell," *J. Electrochem. Soc*, **140**(6), 1526 (1993).
8. M. Doyle and J. Newman, "The use of Mathematical Modeling in the design of Lithium/Polymer Battery Systems," *Electrochim. Acta*, **40**(13-14), 2191 (1995).
9. K. E. Thomas and J. Newman, "Thermal Modeling of Porous Insertion Electrodes," *J. Electrochem. Soc*, **150**(2), A176 (2003).
10. H. J. Ploehn, P. Ramadass, and R. E. White, "Solvent Diffusion Model for Aging of Lithium-Ion Battery Cells," *J. Electrochem. Soc*, **151**(3), A456 (2004).
11. A. J. Smith, A. C. Burns, X. Zhao, D. Xiong, and J. R. Dahn, "A High Precision Coulometry Study of the SEI Growth in Li/Graphite Cells," *J. Electrochem. Soc*, **158**(5), A447 (2011).
12. M. B. Pinson and M. Z. Bazant, "Theory of SEI Formation in Rechargeable Batteries: Capacity Fade, Accelerated Aging and Lifetime Prediction," *J. Electrochem. Soc*, **160**(2), A243 (2013).
13. G.-H. Kim, K. Smith, K.-J. Lee, S. Santhanagopalan, and A. Pesaran, "Multi-Domain Modeling of Lithium-Ion Batteries Encompassing Multi-Physics in Varied Length Scales," *J. Electrochem. Soc*, **158**(8), A955 (2011).
14. R. E. Garcia, Y.-M. Chiang, W. C. Carter, P. Limthongkul, and C. M. Bishop, "Microstructural Modeling and Design of Rechargeable Lithium-Ion Batteries," *J. Electrochem. Soc*, **152**(1), A255 (2005).
15. M. Smith, R. E. Garcia, and Q. C. Horn, "The Effect of Microstructure on the Galvanostatic Discharge of Graphite Anode Electrodes in $LiCoO_2$-Based Rocking-Chair Rechargeable Batteries," *J. Electrochem. Soc*, **156**(11), A896 (2009).
16. D. Bedrov, G. D. Smith, and A. C. T. van Duin, "Reactions of Singly-Reduced Ethylene Carbonate in Lithium Battery Electrolytes: A Molecular Dynamics Simulation Study Using the ReaxFF," *J. Phys. Chem. A*, **116**(11), 2978 (2012).
17. M. Safari, M. Morcrette, A. Teyssot, and C. Delacourt, "Multimodal Physics-Based Aging Model for Life Prediction of Li-Ion Batteries," *J. Electrochem. Soc*, **156**(3), A145 (2009).
18. S. K. Rahimian, S. C. Rayman, and R. E. White, "Maximizing the Life of a Lithium-Ion Cell by Optimization of Charging Rates," *J. Electrochem. Soc*, **157**(12), A1302 (2010).

19. L. Cai and R. E. White, "Reduction of Model Order Based on Proper Orthogonal Decomposition for Lithium-Ion Battery Simulations," *J. Electrochem. Soc*, **156**(3), A154 (2009).
20. S. Onori, P. Spagnol, V. Marano, Y. Guezennec, and G. Rizzoni, "A new life estimation method for lithium-ion batteries in plug-in hybrid electric vehicles applications," *Int. J. Power Electronics*, **4**(3), 302 (2012).
21. I. Battiato, D. M. Tartakovsky, A. M. Tartakovsky, and T. Scheibe, "On breakdown of macroscopic models of mixing-controlled heterogeneous reactions in porous media," *Adv. Water Resour.*, **32**(11), 1664 (2009).
22. I. Battiato and D. M. Tartakovsky, "Applicability regimes for macroscopic models of reactive transport in porous media," *J. Contam. Hydrol.*, **120-121**, 18 (2011).
23. F. Boso and I. Battiato, "Homogenizability conditions for multicomponent reactive transport," *Adv. Water Resour.*, **62**, 254 (2013).
24. P. Spagnol, S. Onori, N. Madella, Y. Guezennec, and N. John, "Aging and characterization of li-ion batteries in a hev application for lifetime estimation," in *Adv. Automotive Control, 2010*, 186 (2010).
25. S. P. Neuman and D. M. Tartakovsky, "Perspective on theories of non-Fickian transport in heterogeneous media," *Adv. Water Resour.*, **32**(5), 670 (2009).
26. S. Whitaker, *The Method of Volume Averaging*. Springer, Netherlands, 1999.
27. U. Hornung, *Homogenization and Porous Media*. Springer, New York, 1997.
28. M. A. Peter, "Coupled reaction-diffusion processes inducing an evolution of the microstructure: Analysis and homogenization," *Nonlinear Anal. Theory Methods Appl.*, **70**(2), 806 2009.
29. W. G. Gray and C. T. Miller, "Thermodynamically constrained averaging theory approach for modeling flow and transport phenomena in porous medium systems: 7. Single-phase megascale flow models," *Adv. Water Resour.*, **32**(8), 1121 (2009).
30. J. H. Cushman, L. S. Bennethum, and B. X. Hu, "A primer on upscaling tools for porous media," *Adv. Water Resour.*, **25**(8-12), 1043 (2002).
31. F. Ciucci and W. Lai, "Derivation of Micro/Macro Lithium Battery Models from Homogenization," *Transp. Porous Media*, **88**(2), 249 (2011).
32. J. Groot, *State-of-Health Estimation of Li-ion Batteries: Cycle Life Test Methods*. PhD thesis, Chalmers University of Technology, (2012).
33. E. Finden, "A Homogenized Thermal Model for Lithium Ion Batteries," Master's thesis, Norwegian University of Life Sciences, (2012).
34. Y. Davit, C. G. Bell, H. M. Byrne, L. A. C. Chapman, L. S. Kimpton, G. E. Lang, K. H. L. Leonard, J. M. Oliver, N. C. Pearson, R. J. Shipley, S. L. Waters, J. P. Whiteley, B. D. Wood, and M. Quintard, "Homogenization via formal multiscale asymptotics and volume averaging: How do the two techniques compare?," *Adv. Water Resour.*, **62**, 178 (2013).
35. A. Salvadori, E. Bosco, and D. Grazioli, "A computational homogenization approach for Li-ion battery cells: Part 1 - formulation," *J. Mech. Phys. Solids*, **65**, 114 (2014).
36. G. B. Less, J. H. Seo, S. Han, A. M. Sastry, J. Zausch, A. Latz, S. Schmidt, C. Wieser, D. Kehrwald, and S. Fell, "Micro-Scale Modeling of Li-Ion Batteries: Parameterization and Validation," *J. Electrochem. Soc*, **159**(6), A697 (2012).
37. E. Martinez-Rosas, R. Vasquez-Medrano, and A. Flores-Tlacuahuac, "Modeling and simulation of lithium-ion batteries," *Comput. Chem. Eng.*, **35**(9), 1937 (2011).
38. C. Taborelli, S. Onori, S. Maes, P. Sveum, S. Al-Hallaj, and N. Al-Khayat, "Advanced battery management system design for SOC/SOH estimation for e-bikes applications," in *International Journal of Powertrains*, May (2015).
39. S. J. Moura, N. A. Chaturvedi, and M. Krstic, "Adaptive Partial Differential Equation Observer for Battery State-of-Charge/State-of-Health Estimation Via an Electrochemical Model," *J. Dyn. Sys., Meas., Control*, **136**(1), (2013).
40. H. Arunachalam, S. Onori, and I. Battiato, "Temperature-dependent multiscale-dynamics in Lithium-Ion battery electrochemical models," in *American Control Conference (ACC), 2015*, July (2015).
41. S. J. Moura, N. A. Chaturvedi, and M. Krstic, "PDE estimation techniques for advanced battery management systems - part i: SOC estimation," in *American Control Conference (ACC), 2012*, 559 (2012).
42. S. J. Moura, N. A. Chaturvedi, and M. Krstic, "PDE estimation techniques for advanced battery management systems - part ii: SOH identification," in *American Control Conference (ACC), 2012*, 566 (2012).
43. N. A. Chaturvedi, R. Klein, J. Christensen, J. Ahmed, and A. Kojic, "Algorithms for Advanced Battery-Management Systems," *IEEE Control Syst. Mag.*, **30**(3), 49 (2010).
44. S. Santhanagopalan, Q. Guo, P. Ramadass, and R. White, "Review of models for predicting the cycling performance of lithium ion batteries," *J. Power Sources*, **156**(2), 620 (2006).
45. L. Zhang, L. Wang, G. Hinds, C. Lyu, J. Zheng, and J. Li, "Multi-objective optimization of lithium-ion battery model using genetic algorithm approach," *J. Power Sources*, **270**, 367 (2014).
46. S. Basu, R. S. Patil, S. Ramachandran, K. S. Hariharan, S. M. Kolake, T. Song, D. Oh, T. Yeo, and S. Doo, "Non-isothermal electrochemical model for lithium-ion cells with composite cathodes," *J. Power Sources*, **283**, 132 (2015).
47. M. Xu, Z. Zhang, X. Wang, L. Jia, and L. Yang, "A pseudo three-dimensional electrochemical-thermal model of a prismatic $LiFePO_4$ battery during discharge process," *Energy*, **80**, 303 (2015).
48. K. Somasundaram, E. Birgersson, and A. S. Mujumdar, "Model for a bipolar Li-ion battery module: Automated model generation, validation and verification," *Appl. Math. Comput.*, **219**, 2231 (2012).
49. G. M. Goldin, A. M. Colclasure, A. H. Wiedemann, and R. J. Kee, "Three-dimensional particle-resolved models of li-ion batteries to assist the evaluation of empirical parameters in one-dimensional models," *Electrochim. Acta*, **64**, 118 (2012).
50. J. Christensen, V. Srinivasan, and J. Newman, "Optimization of lithium titanate electrodes for high-power cells," *J. Electrochem. Soc*, **153**(3), A560 (2006).
51. Q. Sun, Q. Wang, X. Zhao, J. Sun, and Z. Lin, "Numerical study on lithium titanate battery thermal response under adiabatic condition," *Energy Convers. Manage.*, **92**, 184 (2015).
52. P. Albertus, J. Christensen, and J. Newman, "Experiments on and Modeling of Positive Electrodes with Multiple Active Materials for Lithium-Ion Batteries," *J. Electrochem. Soc*, **156**(7), A606 (2009).
53. L. Cai and R. E. White, "An Efficient Electrochemical-Thermal Model for a Lithium-Ion Cell by Using the Proper Orthogonal Decomposition method," *J. Electrochem. Soc*, **157**(11), A1188 (2010).
54. S.-C. Chen, Y.-Y. Wang, and C.-C. Wang, "Thermal Analysis of Spirally Wound Lithium Batteries," *J. Electrochem. Soc*, **153**(4), A637 (2006).
55. N. Baba, H. Yoshida, M. Nagaoka, C. Okuda, and S. Kawauchi, "Numerical simulation of thermal behavior of lithium-ion secondary batteries using the enhanced single particle model," *J. Power Sources*, **252**, 214 (2014).
56. Y. Ye, Y. Shi, and A. A. O. Tay, "Electro-thermal cycle life model for lithium iron phosphate battery," *J. Power Sources*, **217**, 509 (2012).
57. M. Guo, G. Sikha, and R. E. White, "Single-Particle Model for a Lithium-Ion Cell: Thermal Behavior," *J. Electrochem. Soc*, **158**(2), A122 (2011).
58. P. Gambhire, N. Ganesan, S. Basu, K. S. Hariharan, S. M. Kolake, T. Song, D. Oh, T. Yeo, and S. Doo, "A reduced order electrochemical thermal model for lithium ion cells," *J. Power Sources*, **290**, 87 (2015).
59. G. Ning and B. N. Popov, "Cycle Life Modeling of Lithium-Ion Batteries," *J. Electrochem. Soc*, **151**(10), A1584 (2004).
60. M. Guo and R. E. White, "Thermal Model for Lithium Ion Battery Pack with Mixed Parallel and Series Configuration," *J. Electrochem. Soc*, **158**(10), A1166 (2011).
61. J. Park, J. H. Seo, G. Plett, W. Lu, and A. M. Sastry, "Numerical Simulation of the Effect of the Dissolution of $LiMn_2O_4$ Particles on Li-Ion Battery Performance," *J. Electrochem. Soc*, **14**(2), A14 (2011).
62. L. O. Valoen and J. N. Reimers, "Transport Properties of $LiPF_6$-Based Li-Ion Battery Electrolytes," *J. Electrochem. Soc*, **152**(5), A882 (2005).
63. I. Battiato, D. M. Tartakovsky, A. M. Tartakovsky, and T. D. Scheibe, "Hybrid models of reactive transport in porous and fractured media," *Adv. Water Resour.*, **43**(4), 1140 (2011).
64. J. L. Auriault and P. M. Adler, "Taylor dispersion in porous media: Analysis by multiple scale expansions," *Adv. Water Resour.*, **18**(4), 217 (1995).
65. Y. Efendiev, O. Iliev, and V. Taralova, "Upscaling of an isothermal Li-ion battery model via the Homogenization Theory," *Scientific Report of Fraunhofer ITWM*, **230**, (2013).